Title

Validation of an arterial constitutive model accounting for collagen content and crosslinking

Permalink

https://escholarship.org/uc/item/1w18d45h

Authors

Tian, Lian
Wang, Zhijie
Liu, Yuming
et al.

Peer reviewed

Validation of an Arterial Constitutive Model Accounting for Collagen Content and Crosslinking

Lian Tian[1], **Zhijie Wang**[1], **Yuming Liu**[2], **Jens C. Eickhoff**[3], **Kevin W. Eliceiri**[2], and **Naomi C. Chesler**[1,*]

[1]Department of Biomedical Engineering, University of Wisconsin-Madison, Madison, Wisconsin

[2]Laboratory for Optical and Computational Instrumentation, University of Wisconsin-Madison, Madison, Wisconsin

[3]Department of Biostatistics and Medical Informatics, University of Wisconsin-Madison, Madison, Wisconsin

Abstract

During the progression of pulmonary hypertension (PH), proximal pulmonary arteries (PAs) increase in both thickness and stiffness. Collagen, a component of the extracellular matrix, is mainly responsible for these changes via increased collagen fiber amount (or content) and crosslinking. We sought to differentiate the effects of collagen content and cross-linking on mouse PA mechanical changes using a constitutive model with parameters derived from experiments in which collagen content and cross-linking were decoupled during hypoxic pulmonary hypertension (HPH). We employed an eight-chain orthotropic element model to characterize collagen's mechanical behavior and an isotropic neo-Hookean form to represent elastin. Our results showed a strong correlation between the material parameter related to collagen content and measured collagen content ($R^2 = 0.82$, $P < 0.0001$) and a moderate correlation between the material parameter related to collagen crosslinking and measured crosslinking ($R^2 = 0.24$, $P = 0.06$). There was no significant change in either the material parameter related to elastin or the measured elastin content from histology. The model-predicted pressure at which collagen begins to engage was ~25 mmHg, which is consistent with experimental observations. We conclude that this model may allow us to predict changes in the arterial extracellular matrix from measured mechanical behavior in PH patients, which may provide insight into prognoses and the effects of therapy.
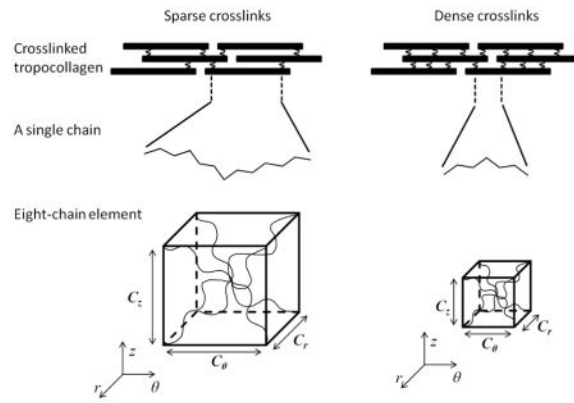
Graphical Abstract

---

*Corresponding author: Department of Biomedical Engineering, University of Wisconsin-Madison, 2146 ECB, 1550 Engineering Drive, Madison, WI 53706-1609, USA, chesler@engr.wisc.edu, Tel: 608-265-8920, Fax: 608-265-9239.

Disclosures

No conflicts of interest are declared by the author(s).

Collagen fibers in large pulmonary artery are characterized by an eight-chain element model with n and N being the tropocollagen chain density per unit volume and the number of subunits per chain, respectively. Because smaller N indicates denser crosslinks, $n \cdot N$ and N are correlated to collagen content and collagen crosslinking, respectively.

Keywords

hydroxyproline; pyridinoline; modeling; β-aminopropionitrile (BAPN); large pulmonary artery

Introduction

During the progression of pulmonary hypertension (PH), proximal pulmonary arteries (PAs) become stiffer due to extrinsic and intrinsic remodeling including arterial wall thickening (extrinsic remodeling) and increased elastic modulus (intrinsic remodeling) [1–7]. Arterial stiffening can increase right ventricular (RV) afterload, which causes RV hypertrophy and eventually RV failure [8–14]. Clinical studies have found that proximal PA stiffness and its inverse, compliance, are strongly related to mortality in patients with PH [12,15–20]. Therefore, it is important to understand the extrinsic and intrinsic changes in proximal PAs that are responsible for stiffening in PH.

Many mechanical testing methods including uniaxial, planar biaxial and pressure-inflation tests have been used to characterize the extrinsic and intrinsic, or more generally, mechanical properties of proximal PAs and their components [1,3,4,6,21–23]. The role of smooth muscle cell activity in proximal PA remodeling, without experimental or pharmacological activation, appears minimal [23,24]. Instead, changes in the extracellular matrix (e.g., elastin and collagen) can be dramatic. Elastin, which bears most of the mechanical load in the low stretch region [4,25–27], was found to increase elastic modulus significantly in a neonatal calf model of hypoxic pulmonary hypertension (HPH) and to contribute importantly to increased arterial stiffness [4]. In the adult mouse model of HPH, however, elastin was not found to change significantly; instead, collagen accumulation was found to correlate to the PA elastic modulus in the physiological strain range [3,5]. The effect of collagen on the mechanical properties of proximal PAs has thus been a focus of recent studies [3,5,23,28,29]. In several studies, collagen content has been found to correlate well with the arterial elastic modulus in the physiological strain range [3,5,28,29]. In

addition, a recent study by our group showed that collagen crosslinking is better correlated to elastic modulus at high stretch levels than collagen content [23].

Increased collagen crosslinking increases the elastic modulus of collagen fibers [30–34]. At the microscopic level, collagen crosslinking can restrict the slippage between collagen fibrils and between tropocollagen molecules, which results in early stretching of tropocollagen molecules [35]. Stretching itself stiffens tropocollagen molecules, which in turn leads to a stiffer collagen fiber. Therefore, crosslinks also play an important role in the mechanical behavior of collagen fibers and thus artery. The separate effects of collagen content and crosslinking on mechanical behavior were experimentally studied recently by our group [23,29]. In these studies, we utilized a novel experimental design to decouple changes in collagen content from crosslinking during the progression of HPH in mice. In particular, transgenic mice with collagen Type I resistant to collagenase degradation were used, and when exposed to chronic hypoxia, the PAs of both homozygous mutant and wildtype mice increased collagen content and crosslinking. However, when treated with the antifibrotic agent β-aminopropionitrile (BAPN) during the hypoxic exposure, crosslink formation was prevented and thus content and cross-linking were decoupled. Using this experimental approach, we found that the arterial elastic modulus correlated well with collagen content below 25 mmHg and crosslinking above 25 mmHg.

These results motivated us to use a constitutive model to differentiate the mechanical effects of changes in collagen content and crosslinking. Such a constitutive model can be used to study the effects of biology on mechanics broadly and may be used to predict the biological changes responsible for mechanical changes evident during the progression of disease. Many constitutive models, either phenomenological or structural, have been proposed to describe the mechanical properties of large elastic arteries. The phenomenological approach with polynomial, exponential or logarithmic function [36–39] captures hyperelastic behavior, but does not provide information about arterial material and structure. Structural strain-energy functions (SEFs) with terms representing elastin and collagen have been used as well [21,26,40,41], but none of these models has material parameters related to collagen crosslinking. One model that does effectively capture the effects of fiber crosslinking is an eight-chain isotropic element model that uses statistical mechanics to model the hyperelastic behavior of macromolecules [42]. This model was later revised to an orthotropic model by Bischoff and co-workers [43] and has then been applied to the large PAs of a rat model of HPH to predict crosslinking from the PA mechanical behavior [7]. However, the latter study did not distinguish between elastin and collagen content or crosslinking.

In this study, we adapted the microstructurally based eight-chain orthotropic element model used by Bischoff and co-workers [43] by adding a neo-Hookean form to represent elastin fibers and then investigated the revised model's ability to distinguish the effects of collagen content from collagen crosslinking on the elastic modulus of PAs during HPH. We first found model parameters for collagen content and crosslinking by fitting to experimental stress-stretch data. We then studied the correlations between the model parameters and the measured collagen content and crosslinking in the experimental groups with decoupled collagen content and crosslinking [23,29]. Finally, we compared the model-predicted collagen engagement or transition stretch to that obtained with two previously established

methods and then used the model-predicted transition stretch to interpret the experimental observations of pressure-dependent contributions of collagen content and crosslinking to arterial mechanics [23,29].

Materials and Methods

Materials

Data used to populate the model were derived from animals experiments that have been previously reported [23,29]. Briefly, homozygous mutant (Col1a1$^{R/R}$) and wildtype (Col1a1$^{+/+}$) mice were exposed to 10 days of chronic hypoxia to induce PH. In the mutant animals, the alpha-1 subunit of type I collagen is resistant to degradation whereas in the wildtype animals, collagen type I is degraded normally. Half of the animals exposed to chronic hypoxia were also treated with BAPN, which prevents new crosslink formation. Additional mutant and wildtype mice without any hypoxia exposure or treatment were used as controls.

Isolated Vessel Pressure-inflation Test

Details of the pressure-inflation test are available elsewhere [23,29]. Briefly, extralobar left pulmonary arteries (LPAs) were harvested from mice post-euthanasia and mounted on glass microcannulas in an isolated vessel mechanical testing chamber with an optical viewing window directly below the artery for transillumination microscopy measurement of diameter. Calcium- and magnesium-free PBS medium was used for perfusion and superfusion to ensure the passive state of smooth muscle cells. The distance between the microcannulas was increased to stretch the vessels longitudinally to a near in vivo stretch. All tests were performed at a fixed longitudinal stretch ratio of 140%, a frequently used estimate of in vivo PA stretch and only pressure-circumferential deformation data (not axial force-length data) were obtained. A steady flow pump (LSI; Burlington, VT) with closed loop feedback control was used to pressure-inflate the arteries at transmural pressures of 5, 10, 15, 20, 25, 30, 35, 40 mmHg. LPA outer diameter and transmural pressure were simultaneously recorded.

Calculations: Stretch and Stress

To obtain circumferential stress-stretch curves, the simultaneously obtained pressure-outer diameter (OD) data were used. Note that due to residual strain, the artery under no-load state is under tension at the outer wall [27,44,45]. A combination of a longitudinal stretch (140% in this study) and a small intramural pressure can result in an approximate stretch-free state at the outer wall of the artery [27]. Therefore, the OD at 5 mmHg (OD$_5$) was taken as the reference state as in previous studies [5,23,29] such that the circumferential stretch was approximated as $\lambda = OD/OD_5$. The arterial wall volume was calculated using the optically measured inner diameter (ID) and OD at 40 mmHg and the longitudinal stretch. Assuming incompressibility, the ID and arterial wall thickness (h) at different pressures were then calculated. For a thin-walled vessel, which is an appropriate assumption for mouse LPA ($h/ID = 0.096 \pm 0.005$ for all vessels at the no-load state as measured from histology), the circumferential Cauchy stress was estimated as

$$\sigma = \frac{P \cdot r}{h}, \quad (1)$$

where P is the pressure, and *r* and *h* are the inner radius ($r = ID/2$) and thickness of the artery at pressure P, respectively. Details of the calculation can be found in previous studies [23,29].

Calculations: Arterial Constitutive Model

To model the mechanical behavior of the proximal PAs, we ignored the contribution of the passive smooth muscle cells and considered only the extracellular matrix components (elastin and collagen). Note that even in physiological saline solution, the effects of the smooth muscle cells in the proximal PAs on mechanical properties have been found to be minimal [23,24].

A two-term structural strain-energy function was adopted [26]

$$\psi = \psi_{\text{elastin}} + \psi_{\text{collagen}}, \quad (2)$$

where the first term on the right hand side is associated with elastin and the second term with collagen. For elastin, an isotropic neo-Hookean form was used [26,40,46,47]

$$\psi_{\text{elastin}} = G(I_1 - 1)/2, \quad (3)$$

where *G* is the shear modulus of elastin and $I_1 = 2trE + 3$ is the first invariant of the Green-Lagrange strain tensor, *E*.

To investigate the separate effects of collagen content and crosslinking, we employed the microstructurally-based eight-chain orthotropic element model to characterize the collagen fibers' overall mechanical behavior, assuming the collagen fibers are oriented in all three dimensions without specifying the dominant orientation or symmetry of the fibers. Biologically, collagen fibers are assembled from collagen fibrils, which are formed by tropocollagen molecules crosslinked to each other; each tropocollagen molecule consists of three helical polypeptide chains, each polypeptide chain is characterized by a repeating amino acid motif that contains hydroxyproline (Figure 1A). In the model, eight identical chains make up an element. A single chain in the eight-chain element represents a single tropocollagen molecule section between two neighboring crosslinks. The length of each chain depends on the number of repeating amino acid motifs, or subunits, in a section of tropocollagen between neighboring crosslinks. The parameter *N* represents the number of subunits per chain (Figure 1B). The strain energy from collagen fibers is the sum of the entropy of all tropocollagen molecules and the repulsion between them:

$$\psi_{\text{collagen}} = \psi_0 + \frac{nk\Theta}{4} N \sum_{i=1}^{4} \left[\frac{\rho^{(i)}}{N} \beta_\rho^{(i)} + \ln \frac{\beta_\rho^{(i)}}{sinh\beta_\rho^{(i)}} \right] - \frac{nk\Theta}{4} \frac{\beta_P}{\sqrt{N}} \ln \left(\lambda_r^{C_r^2} \lambda_\theta^{C_\theta^2} \lambda_z^{C_z^2} \right) \quad (4)$$

as in [43] where λ_θ, λ_z and λ_r and are the stretch in the circumferential (θ), longitudinal (*z*) and radial (*r*) directions (Figure 1B). No shear deformation was considered in this study.

ψ_0 is a constant related to the non-zero entropy of the undeformed chains in the model; the second term on the right is the change of entropy due to the deformation (or stretching) of chains with non-Gaussian (Langevin) statistics to describe a single chain; and the last term on the right is the strain energy due to repulsion between chains. This repulsion is necessary to establish a stress-free state at the chains' resting condition and thus to prevent the entropic collapse of the unit element [43,48]. The parameter n is the chain density per unit volume (note that there are eight chains per unit element, as shown in Figure 1B), $k = 1.38 \cdot 10^{-23}$ J/K is Boltzmann's constant, $\Theta = 298$ K is the absolute temperature. Note that the section of the tropocollagen molecule between two neighboring crosslinks could have different lengths. However, the model we adopted here does not consider such differences and assumes all these tropocollagen molecular sections have the same length (i.e., the same N in the model) in a given artery. Details of this model can be found elsewhere [43].

All the length parameters in Eq. (4) are normalized by the length of the repeating amino acid motif, or subunit, in the tropocollagen molecule, which is assumed constant. The geometric lengths of the unit element (parameters C_r, C_θ, and C_z) depend on the length of the eight chains in the element, which in turn depends on the density of crosslinking (Figure 1B). Therefore, the unit element generally does not have unitary volume and the product ($C_r \cdot C_\theta \cdot C_z$) is generally not equal to one. $\rho^{(i)}$ is the normalized deformed length of the chains in the unit element where the superscript i denotes the chain number ($i = 1\ldots8$). Due to symmetry of the unit element, only four chains are used and $\rho^{(i)} = \frac{\sqrt{C_r^2 \lambda_r^2 + C_\theta^2 \lambda_\theta^2 + C_z^2 \lambda_z^2}}{2} (i=1\sim4)$, which is the same for all chains under triaxial deformation (λ_r, λ_θ and λ_z 0). $\beta_\rho^{(i)} = \mathscr{L}^{-1}(\rho^{(i)}/N)$, and $\beta_P = \mathscr{L}^{-1}(P/N)$, where $\mathscr{L}(x) = \coth x - \frac{1}{x}$ is the Langevin function, β is the inverse Langevin function, and $P = \frac{\sqrt{C_r^2 + C_\theta^2 + C_z^2}}{2}$ is the normalized undeformed chain length in the unit element. Assuming the undeformed length of a chain is equal to its root mean square length [49,50], $N = P^2 = (C_r^2 + C_\theta^2 + C_z^2)/4$.

Since N is the number of the repeating subunits in a single chain in the element, a larger N corresponds to a longer chain with fewer crosslinks and more extensibility, which indicates a more compliant collagen fiber and artery. Therefore, N was expected to be inversely related to the collagen crosslinking and we used N as the material parameter to be correlated to collagen crosslinking. In addition, because N corresponds to chain length, it is also related to collagen content. In particular, a longer chain has more repeating subunits [35]. Thus, higher N indicates more collagen. The parameter n, which is the number of chains per unit volume (and $n/8$ is the number of model elements per unit volume), is also related to collagen content; higher n indicates more collagen independent of N. Therefore, we used $n \cdot N$ as the material parameter related to collagen content per unit volume. Collagen content and crosslinking per unit volume are available experimentally; content from a biochemical hydroxyproline (OHP) assay or histological staining for collagen and crosslinking from a biochemical pyridinoline (PYD) assay.

In the original strain-energy function [43], an additional term was proposed for control over the compressibility of the material. Here, the vessel was assumed to be incompressible and a

term that indicates the hydrostatic pressure (*H*) was used in the stress calculation to ensure incompressibility. In particular, the Cauchy stresses are calculated as

$$\sigma_{\theta\theta}=\lambda_\theta^2 \tfrac{\partial\psi}{\partial E_\theta}-H, \quad \sigma_{rr}=\lambda_r^2 \tfrac{\partial\psi}{\partial E_r}-H, \quad (5)$$

For a thin-walled vessel, the radial stress can be assumed zero, i.e., $\sigma_{rr} = 0$ [26]. Therefore, the circumferential stress can be determined by solving the radial stress for *H* and substituting this term back into the circumferential stress term as

$$\sigma_{\theta\theta}=\lambda_\theta^2 \tfrac{\partial\psi}{\partial E_\theta}-\lambda_r^2 \tfrac{\partial\psi}{\partial E_r}=G(\lambda_\theta^2-\lambda_r^2)+\tfrac{nk\Theta C_\theta^2}{4}\left(\tfrac{\lambda_\theta^2\beta_\rho}{\rho}-\tfrac{\beta_P}{\sqrt{N}}\right)-\tfrac{nk\Theta C_r^2}{4}\left(\tfrac{\lambda_r^2\beta_\rho}{\rho}-\tfrac{\beta_P}{\sqrt{N}}\right). \quad (6)$$

The parameters C_θ and C_z indicate the collagen fibers' mechanical contribution to the circumferential and longitudinal directions, respectively. A larger value indicates a larger elastic modulus in that direction compared to the other at the same strain range, and $C_\theta = C_z$ indicates transverse isotropy. Since these two parameters are related to collagen fiber distribution, we harvested LPA and RPA from an additional set of mutant and wildtype mice (control and exposed to 10 days of chronic hypoxia) and imaged collagen fiber orientation at a no-load state with a multi-photon microscope via the second harmonic generating (SHG) signals as described previously [51,52]. The orientation of collagen fibers was quantified using custom software [CT-FIRE, developed in the Laboratory for Optical and Computational Instrumentation, UW-Madison ([52]; LOCI @ http://loci.wisc.edu/software/ctfire)]. Our results show that collagen fibers were distributed in all directions in the circumferential-longitudinal plane with the greatest number of collagen fibers oriented in the circumferential direction (See Appendix A). This indicates that PA is stiffer in the circumferential direction than all other directions in this circumferential-longitudinal plane if all the collagen fibers have exactly the same mechanical properties and that the parameter C_θ should be larger than C_z. Nevertheless, previous modeling studies on calf and rat proximal PAs suggested nearly transversely isotropic behavior [21]. Since axial force-length data were not available, we assumed that the PA is transversely isotropic, i.e., the mechanical properties in the circumferential and longitudinal directions are the same, which forces the parameters $C_\theta = C_z$.

Next, Eq. (6) was fit to the experimentally-obtained circumferential stress-stretch curves to find the parameters *G*, *n*, C_θ (or C_z) and C_r for each mouse LPA. Several sets of initial values for the parameters were tried to examine the convergence of the parameters. The best fit was identified via nonlinear regression with Levenberg-Marquardt algorithm by minimizing the mean square error between experimental and model-predicted data, i.e., $\frac{1}{M}\sum_{i=1}^{M}\left(\sigma_i^{\mathrm{mod}}-\sigma_i^{\mathrm{exp}}\right)^2$, where M is the number of data points of the measured stress-stretch curve, and σ_i^{mod} and σ_i^{exp} are the model-predicted and experimentally measured stresses of a point, respectively. The termination tolerance on both the residual function and parameters was set to be 10^{-6}. The goodness-of-fit was characterized by the pseudo R-square, which is the square correlation between the model-predicted and the experimentally measured

stresses [53], i.e., $R^2 = \frac{\sum_{i=1}^{M} \left(\sigma_i^{\text{mod}} - \overline{\sigma^{\text{mod}}}\right)\left(\sigma_i^{\text{exp}} - \overline{\sigma^{\text{exp}}}\right)}{\sum_{i=1}^{M} \left(\sigma_i^{\text{exp}} - \overline{\sigma^{\text{exp}}}\right)^2 \sum_{i=1}^{M} \left(\sigma_i^{\text{mod}} - \overline{\sigma^{\text{mod}}}\right)^2}$, where $\overline{\sigma^{\text{mod}}}$ and $\overline{\sigma^{\text{exp}}}$ are the average model-predicted and experimentally measured stresses, respectively. All these calculations were performed with a custom-written Matlab code (Matlab, Mathworks Inc., Natick, MA, USA) using the *lsqnonlin* subroutine.

Once the coefficients for the constitutive model were obtained, we sought to predict the collagen transition stretch by examining the individual chain extension in the unit element. The probability of the most probable link angle distribution in an individual chain can be described by the Langevin statistics [42,54] and the force or stress of the chain is related to the inverse Langevin function, which is seen in Eq. (6). As a chain deforms, the chain length (ρ) approaches the fully extended length, i.e., the extension ratio $\rho/N \to 1$, and the inverse Langevin function increases approximately linearly when $\rho/N < 0.8$ and nonlinearly and dramatically around $\rho/N = 0.9$ as seen in Figure 2A. The approximately linear behavior in the stretch region when $\rho/N < 0.8$ represents the tropocollagen molecular behavior at an initial state in which molecular slippage occurs. As the chain's stretch increases beyond this region, crosslinking restricts the molecular slippage and causes a transition region around $\rho/N = 0.9$ and a sharp increase when $\rho/N > 0.9$. Therefore, we chose $\rho/N = 0.9$ as the collagen transition point. This leads to $\frac{1}{2} \sqrt{C_r^2 \lambda_r^2 + C_\theta^2 \lambda_\theta^2 + C_\theta^2 \lambda_\theta^2} / \frac{1}{4} \left(C_r^2 + C_\theta^2 + C_z^2\right) = 0.9$. With longitudinal stretch $\lambda_z = 1.4$, radial stretch λ_r expressed as a function of longitudinal and circumferential stretch from the incompressibility condition ($\lambda_r \lambda_\theta \lambda_z = 1$), and the parameters C_r and $C_\theta = C_z$ obtained from model fitting, the collagen transition stretch (λ_T^{mod}) in the circumferential direction can be calculated. An example of the stress-stretch curve of an LPA and its transition point predicted from the model is shown in Figure 2B. As the stretch increases above the transition point, the stresses (both collagen and the total) increase dramatically, which occurs due to the locking of tropocollagen molecules or engagement of collagen fibers.

In the absence of a direct measure of collagen transition stretch, we compared the model-predicted engagement stretch to the transition stretch estimated by two previously established methods. One method used the intersection point of the two lines that best fit the low and high stretch regions of the stress-stretch curve as the transition point [24,29]. The other method used the maximum curvature point of the arterial stress-stretch curve to indicate the transition point [4,55]. We followed the latter procedure by fitting a 9th-order polynomial to the arterial stress-stretch curve. Because we only had eight data points in the experimental stress-stretch curve, we interpolated the data at equal intervals which resulted in a total of twenty-two data points. The new stress-stretch curve including the interpolated data points was then used for the polynomial fitting.

Using the predicted collagen transition stretch, we interpreted previous statements of pressure-dependent contributions of collagen content and crosslinking to arterial mechanics. Since the arterial elastic modulus was found to correlate well to measured collagen content in the pressure range of 10~25 mmHg but to measured crosslinking over the pressure range of 10~40 mmHg [23,29], we compared the experimental circumferential stretch at 25 and 40

mmHg (λ_{P}) to the collagen transition stretch predicted from model ($\lambda_{\text{T}}^{\text{mod}}$) and calculated the differences as $\left(\lambda_{\text{P}} - \lambda_{\text{T}}^{\text{mod}}\right) / \lambda_{\text{T}}^{\text{mod}}$. We also examined whether collagen crosslinking was likely to be a dominating factor in the arterial elastic modulus above 25 mmHg if collagen engagement begins around 25 mmHg.

Biochemical Assays and Histology

To correlate material parameters in the model to biological properties, available measurements of collagen content and crosslinking from histology and biochemical assays were used. In the set of mice from which static mechanical data were used for modeling [23], LPAs were stained with hematoxylin and eosin (H&E) and Verhoeff's Van Gieson (VVG) and photographed for geometric and histology analysis, and right PAs (RPAs) were used to measure crosslinking via pyridinoline (PYD). In another set of mice of the same genotypes and exposed to the same conditions [29], LPAs were used to measure collagen content via hydroxyproline (OHP).

From the histological images of VVG-stained LPAs, we examined the elastin content. From the histological images of H&E-stained LPAs, we measured the arterial wall thickness and inner wall circumference to calculate the arterial wall cross-sectional area (CSA). In the biochemical assays, the wet weights were not measured for either LPA or RPA. Therefore, to obtain collagen content and crosslinking in a unit element, we assumed that the material density is the same for all the vessels, the lengths of all the LPAs or RPAs used for collagen content study (OHP) or crosslinking study (PYD) are the same, and the collagen crosslinking in the LPA is proportional (by volume) to that in RPA. With these assumptions, the group average CSAs rather than volumes were then used to normalize collagen content and crosslinking. The standard errors of the parameters in each group were propagated to the normalized collagen content and crosslinking [56].

Statistics

All the data are presented as mean ± SE unless specified otherwise. For each mouse strain, comparisons between groups were performed by one-way analysis of variance (ANOVA) with Tukey's HSD post comparisons using R software version 2.15 (www.r-project.org). The correlations between the groups for measured collagen content, crosslinking and material parameters in the arterial constitutive model were evaluated using a parametric bootstrap approach based on a bivariate normal distribution model [57]. A bootstrap sample size of M = 10,000 was used for each calculation. Bland-Altman analysis [58] was conducted to evaluate the reliability between collagen transition stretch estimated from different methods. Paired t-test was performed to compare the experimentally obtained stretch at 25 and 40 mmHg and the model-predicted transition stretch. All *P*-values were two-sided and *P*-values less than 0.05 were used to define statistical significance.

Results

Table 1 summarizes the measured cross-sectional area in LPA and the normalized collagen content (OHP) and crosslinking (PYD) by CSA. The cross-sectional area did not change

significantly after chronic hypoxia with or without BAPN treatment. The normalized collagen content and crosslinking had the same trends between groups as the non-normalized data. Hypoxia increased collagen content and crosslinking in both strains of mice. With BAPN treatment, in the wildtype mice, the non-crosslinked collagen fibers were degraded such that the increase of collagen content was limited compared to the untreated group; in the mutant mice, however, the crosslinking was at baseline levels and the total collagen content remained elevated. The elastin content was not significantly different between groups (data not shown).

The average Cauchy stress-stretch curves for each group of $Col1a1^{+/+}$ and $Col1a1^{R/R}$ mice are shown in Figure 3. In general, chronic hypoxia caused an increase in the arterial elastic modulus in the physiological strain range, as indicated by the increase in the tangential slope of the stress-stretch curve, and BAPN treatment limited such increase.

Table 2 summarizes the estimated material parameters of the constitutive model. The fitting process showed that the parameter C_r is very close to zero and several orders of magnitude smaller than the parameter $C_\theta = C_z$. Therefore, we performed a second fitting with $C_r = 0$ and let the other parameters G, n and $C_\theta = C_z$ be free. Parameter values found with different sets of initial values were not significantly different. The root-mean-square error had a range from 0.12 to 1.47 kPa with an average of 0.57 ± 0.35 kPa (mean $\pm$ SD). Goodness-of-fit was very good ($R^2 > 0.998$) for all samples and setting $C_r = 0$ did not change the fitted parameter values (G, n and $C_\theta = C_z$). No statistically significant difference was found for any parameter fit to the Normoxia, Hypoxia or Hypoxia+BAPN data for either $Col1a1^{+/+}$ or $Col1a1^{R/R}$ mice. However, G showed a moderate decrease and both n and $n \cdot N$ tended to increase in both $Col1a1^{+/+}$ and $Col1a1^{R/R}$ mice exposed to hypoxia. BAPN treatment did not alter the moderate decrease in G or the elevation in n or $n \cdot N$ for $Col1a1^{+/+}$ mice; however, it prevented the decrease in G and the increase in n or $n \cdot N$ for $Col1a1^{R/R}$ mice.

No strong correlation was evident between group averages of normalized collagen content (OHP/CSA); the material parameter related to collagen content ($n \cdot N$) when all groups are included is shown in Figure 4A (no trend line is plotted). However, when the $Col1a1^{R/R}$ Hypoxia+BAPN group was excluded (circled in Figure 4A), we found a strong positive correlation between normalized collagen content and the parameter $n \cdot N$ for the other five groups ($R^2 = 0.82$, $P < 0.0001$). A weak to moderate, non-significant or marginally significant, negative correlation [59] was observed between group averages of normalized crosslinking (PYD/CSA) and the material parameter related to crosslinking (N) regardless of whether the $Col1a1^{R/R}$ Hypoxia+BAPN group (circled in Figure 4B) was included in the correlation analysis ($R^2 = 0.16$, $P = 0.18$ and $R^2 = 0.24$, $P = 0.06$ with the $Col1a1^{R/R}$ Hypoxia+BAPN group excluded and included, respectively; Figure 4B&C).

Figure 5A shows the model-predicted collagen transition stretch in the circumferential direction with fixed longitudinal stretch ($\lambda_z = 1.4$). No significant difference was found between Normoxia, Hypoxia and Hypoxia+BAPN groups for either $Col1a1^{+/+}$ or $Col1a1^{R/R}$ mice. Figure 5B presents the Bland-Altman plot for the collagen transition stretch from model prediction and the two-line intersection point method. The model prediction has a bias (or average difference) of 0.023 with the limits of agreement at two standard deviations

(SDs) of the difference at 0.35 compared with this method, and there are only two outliers. With the Col1a1$^{R/R}$ Hypoxia+BAPN group excluded, the bias and two SDs are 0.033 and 0.36, respectively. The maximum curvature point method showed all transition stretch was less than 1.2, i.e., it occurred at the foot of the stress-stretch curve, which was not reasonable. We also tried lower order polynomials (4th- and 5th- order) for the fitting to the stress-stretch curve, which also resulted in a transition stretch less than 1.2. Thus we disregarded these results.

The comparison between the experimentally-obtained circumferential stretch at 25 and 40 mmHg from the inflation test and the collagen transition stretch predicted from model for each artery is shown in Figure 6. The experimentally-obtained stretch at 25 mmHg is smaller than or around the model-predicted transition stretch for most arteries (Figure 6A). In contrast, the experimentally-obtained stretch at 40 mmHg is larger than or around the model-predicted transition stretch for most arteries (Figure 6B). The differences between the experimentally obtained stretch at 25 and 40 mmHg and the model-predicted transition stretch are -2.4% ± 2.0% ($P = 0.10$) and 7.2% ± 1.3% ($P < 0.00001$), respectively. If the Col1a1$^{R/R}$ Hypoxia+BAPN group is excluded, these difference are -2.7% ± 1.8% ($P = 0.15$) and 6.8% ± 1.2% ($P < 0.00001$) at 25 and 40 mmHg, respectively.

A limited sensitivity study of the material parameters was performed. Since we are more interested in the effect of collagen than elastin on the mechanical properties in the current study, we fixed the material parameter for elastin, $G = 3.7$ kPa, an average of all LPAs, and examined the effects of the collagen fiber density (n) and the number of rigid links in each collagen fiber chain (N). To do so, we chose $n = 1, 5$ and 9×10^{23} (n varied from 0.9 to 9.4 $\times 10^{23}$ in the fittings) and let $N = 3.6$. Figure 7A shows that collagen content (represented by $n \cdot N$) affects the stress-stretch relationship mainly at the low stretch region, before collagen engagement (Figure 7A). An important result is that the model-predicted engagement stretch is not a function of n ($\lambda_\mathrm{T}^\mathrm{mod} = 1.97$ for all three cases). To investigate the effect of the predicted number of rigid links in each collagen fiber chain (N), we chose $N = 2.8, 3.9$ and 5.0 (N varied from 2.8 to 5.0 in the fittings) and let $n = 2.9 \times 10^{23}$. As shown in Figure 7B, collagen crosslinking determines collagen engagement stretch ($\lambda_\mathrm{T}^\mathrm{mod} = 1.60, 2.09,$ and 2.48 for $N = 2.8, 3.9$ and 5.0, respectively).

Discussion

In this study, we combined a microstructurally-based hyperelastic model of collagen and a neo-Hookean model of elastin to predict the biological changes in proximal PAs that are responsible for mechanical changes with HPH. The decoupling of collagen content and crosslinking in the experimental design allowed us to investigate the ability of the model to differentiate the mechanical consequences of changes in collagen content distinct from crosslinking. We found an excellent correlation between the material parameter related to collagen content and experimentally measured collagen content, and a weak to moderate negative correlation between the material parameter related to crosslinking and experimentally measured crosslinking in proximal PAs. In addition, we found the model-predicted collagen transition stretch agrees well with previous estimation methods.

Furthermore, by using the model-predicted collagen engagement stretch, we confirmed that collagen content and crosslinking contribute differently to arterial mechanics as a function of pressure, depending on collagen fiber engagement. This paper is the first study to verify material parameters in the constitutive model with measured collagen content and crosslinking. Details of our results are discussed below.

The material parameter, G, which represents the effective elastic modulus of elastin, was not found to be significantly different between groups. Nevertheless, G showed a moderate decrease after hypoxia (Table 2), which is reasonable. In a previous study on the same wildtype and mutant mice [5], the elastin content in mouse PAs did not change significantly with either hypoxia or recovery, which led to no correlation between PA elastic modulus at low stretch and elastin content. Here, we also did not see a significant change in the elastin content from histology. This indicates that not only elastin but also other extracellular components especially collagen contribute to the elastic modulus in the low stretch region. Since collagen content increased after hypoxia, the fractional contribution of elastin to the elastic modulus in the low stretch region decreased. As a result, the material parameter for elastin, G, decreased after hypoxia. With BAPN treatment to prevent crosslinking, the effect of collagen on the mechanical properties was diminished, and collagen played a lesser role in the elastic modulus at low stretch as compared to the hypoxic, untreated group. Thus, elastin contributed relatively more to the elastic modulus at low stretch with BAPN treatment and the effective elastic modulus of elastin (G) increased toward the Normoxia group (Table 2). The congruence between the model predictions and biological data suggest the neo-Hookean model reasonably represents the mechanical behavior of elastin in PAs.

The material parameter, C_r, was found to be zero via the model fitting. This indicates that the three-dimensional unit element (Figure 1) reduces to a two-dimensional (longitudinal-circumferential) plane element and collagen fibers do not contribute to the radial direction. Unfortunately, we have neither mechanical data nor three-dimensional microscopic images directly showing collagen fibers' two-dimensional behavior. Nevertheless, previous studies have suggested that collagen fibers have a planar distribution in human cerebral arteries, calf proximal PAs and rabbit carotid arteries [21,60–62], and several modeling studies have adopted a planar distribution of collagen fibers previously with good results [26,35,41]. The zero value for the material parameter, C_r, is thus believed to be reasonable. Nevertheless, imaging studies on collagen fiber orientation in proximal PAs are required to support the model prediction.

The sensitivity study on the material parameters for collagen indicated that while the number of collagen fibers per unit volume (represented by n) affects the arterial behavior in the low stretch region before collagen engagement and not collagen engagement stretch (Figure 7A), collagen crosslinking (N) does determine collagen engagement stretch (Figure 7B). However, since collagen content is related to both n and N, collagen content also affects collagen engagement stretch. Note that a significant limitation of the model is the assumption that all collagen fibers are crosslinked.

This assumption, and its consequences, may explain why the Col1a1$^{R/R}$ Hypoxia+BAPN group is an outlier in the otherwise strong correlation between experimentally measured

collagen content and model-predicted collagen content $n \cdot N$ (Figure 4A). In the BAPN-treated group, crosslinking of newly secreted tropocollagen molecules was prevented [32,63], and these non-crosslinked tropocollagen molecules were not stable enough to resist degradation in the Col1a1$^{+/+}$ mice [35]. However, in the Col1a1$^{R/R}$ mice, even non-crosslinked and thus non-stable tropocollagen molecules could not be degraded [64]. As a result, the PAs of the Col1a1$^{R/R}$ Hypoxia+BAPN group of mice had both crosslinked and non-crosslinked collagen. Therefore, the mechanical behavior of the PAs from Col1a1$^{R/R}$ Hypoxia+BAPN mice may not be characterized well by the present constitutive model. We conclude that the material parameter ($n \cdot N$) is a strong predictor of collagen content when the majority of the collagen is crosslinked.

Interestingly, this assumption did not appear to affect the correlation between measured crosslinking and the material parameter related to crosslinking (N) (Figure 4B&C). Indeed, this correlation was stronger when the Col1a1$^{R/R}$ Hypoxia+BAPN group was included, likely because non-crosslinked, un-degraded tropocollagen molecules do not contribute significantly to collagen engagement stretch. Nevertheless, this correlation was only moderate and not significant, which may be due to four factors. First, the crosslinks were measured experimentally via pyridinoline (PYD), a type of enzymatic crosslinking that exists in both elastin and collagen fibers, but only collagen crosslinking is modeled. Second, other types of collagen crosslinks such as pyrrole and glycation also exist in arteries [35,65] and contribute to the mechanical properties, and these were not measured. Third, previous studies on rabbit common carotid arteries have found that some collagen fibers engage at low stretch while others engage at high stretch [60,66], and this is attributed to different extensibility of collagen fibers, which is then related to the number of crosslinks and the length between two crosslinks. Such gradual engagement may exist in large PAs. In the constitutive model used here, the length between two crosslinks is assumed to be constant. As a result, all the collagen fibers engage at the same deformation or stretch. Fourth, the current model assumes all collagen fibers are crosslinked whereas some heterogeneity may exist. The introduction of a fraction of crosslinking in the model may provide a better prediction. Despite these model limitations, a moderate negative correlation was found (Figure 4C), suggesting that the parameter N decreases as the measured crosslink density increases to some degree [43].

With material parameters obtained by fitting to the experimental mechanical data, the model can be used to predict some aspects of the arterial mechanical behavior. Collagen fibers are very stiff once engaged, which results in arterial stiffening at high stretch and/or pressure. Therefore, the estimation of collagen engagement or transition stretch or strain is of great interest in the literature. In this study, we attempted to find the transition point from the behavior of a tropocollagen molecule which is described as a chain in the eight-chain element model (Figure 1). Langevin statistics was used to account for the limiting chain extensibility [42] and the inverse Langevin function is thus strongly related to the collagen fiber stress as indicated in Eq. (6). We set the chain extension ratio (ρ/N) to be 0.9 as the transition point since the value of the inverse Langevin function changes dramatically around 0.9 (Figure 2A). The calculated transition stretch at this chain extension ratio also indicates a point at which the collagen stress starts to increase dramatically (Figure 2B).

Therefore, such a calculation of the transition point is believed to be a good approximation. The validity of this approach is further supported by our findings as follows.

First, the estimated transition stretch from the model did not show significant difference between groups for either Col1a1$^{+/+}$ or Col1a1$^{R/R}$ mice. This is not surprising. From Figure 3 for the average stress-stretch curves for all groups, we found that for either Col1a1$^{+/+}$ or Col1a1$^{R/R}$ mice, the three groups (Normoxia, Hypoxia and Hypoxia+BAPN) have similar stress-stretch curves. Therefore, their transition stretch also should not be significantly different from each other. Compared to the Normoxia group, the Hypoxia groups for both Col1a1$^{+/+}$ and Col1a1$^{R/R}$ mice show a leftward-shift of the stress-stretch curve, which indicates the increase of arterial elastic modulus and earlier collagen engagement. With BAPN treatment, the stress-stretch curve in the low stretch region shifted back toward the normoxia values, which indicates similar collagen engagement in the BAPN-treated group. The trends of decreased transition stretch after hypoxia and normalized transition stretch after BAPN treatment were also predicted by the model except for the Col1a1$^{R/R}$ Hypoxia +BAPN group (Figure 5A). Again, the Col1a1$^{R/R}$ Hypoxia+BAPN group may not be described well by the current model and thus the model-predicted collagen transition stretch is not very well correlated to the observation from the stress-stretch curves. Second, the PAs of Col1a1$^{R/R}$ mice exhibited smaller elastic modulus in the physiological strain range than those of the Col1a1$^{+/+}$ mice for all the groups (Normoxia, Hypoxia and Hypoxia+BAPN; Figure 3). Therefore, the transition stretch for Col1a1$^{R/R}$ mice should be larger. This is also seen in our model prediction (Figure 5A).

Third, we compared our model-predicted collagen transition stretch to that obtained with another estimation method, since a direct measurement could not be obtained, and found good agreement (Figure 5B). We tried a third method, the method of maximum curvature, but this gave results that were obviously not correct. Note that the two-line method with which we found good agreement is phenomenological and there is no unique, standard way to define low and high strain regions, which may contribute to the variable differences from the model prediction.

Finally, we examined if the predicted collagen engagement behavior can explain the previous experimental observations of different contributions of collagen content and crosslinking to mechanical behavior. We found that for most LPAs at 25 mmHg, the experimentally obtained stretch is around or less than the model-predicted transition stretch (Figure 6A). Therefore, below 25 mmHg, elastin and the initial elastic modulus of collagen play important roles in arterial elastic modulus. The initial elastic modulus of collagen mainly depends on the amount of collagen. This explains why the overall arterial elastic modulus in the pressure range of 10~25 mmHg was well correlated to collagen content rather than crosslinking [29]. At 40 mmHg, the experimentally obtained stretch for most LPAs is larger than the model-predicted transition (Figure 6B). Therefore, collagen crosslinking becomes more important to arterial elastic modulus at high stretch around 40 mmHg. This explains why the overall arterial modulus in the pressure range of 10~40 mmHg was better correlated to crosslinking than collagen content [23]. Note that the above explanation is true regardless of whether all collagen is crosslinked (i.e., whether the Col1a1$^{R/R}$ Hypoxia+BAPN group was included).

The effects of collagen content and crosslinking on arterial mechanical properties is important to understanding arterial stiffening due to pulmonary hypertension, because both collagen content and crosslinking change significantly with pulmonary hypertension [5,23,28,29] and contribute to the arterial mechanical properties. The model allows us to link the biological changes (e.g., collagen content and crosslinking) to the change of the arterial mechanics. Inversely, the change of arterial mechanics due to hypertension can be expressed in the change of material parameters of the model, and such changes in material parameters provide information on the biological changes. If the model is validated in human PAs, it will be very powerful in clinical studies. In particular, clinically measured PA mechanical behavior, i.e., the in vivo pressure-inner diameter data and the arterial wall thickness via current techniques such as right heart catheterization, echocardiography and intravascular ultrasound [22], could be used in combination with the model to predict PA biological changes, which in turn might be useful to understanding the status of the disease and the efficacy of therapeutic strategies. Moreover, in view of the similar structure and composition of other blood vessels compared to PAs, the model may be successfully applied to other blood vessels.

In addition to the limitations of the model noted above, several experimental limitations are noted in this study. First, due to the small size of the mouse PAs, we were not able to obtain tissue specimen weights or both collagen content and crosslinking from the same tissue. Thus, we could not normalize collagen content and crosslinking by wet weight. As a result, we obtained collagen content from a set of LPAs and crosslinking and cross-sectional area respectively from another set of RPAs and LPAs, and normalized the measured collagen content and crosslinking by the cross-sectional area. In addition, animal-specific correlations could not be performed. Second, pressure-circumferential deformation measurements were obtained at only one longitudinal stretch and without the longitudinal load measured. Without knowledge of the mechanical properties in the longitudinal direction, we assumed transverse isotropy ($C_\theta = C_z$) in the model for both control and PH groups based on the literature and SHG microscopic imaging of the collagen fiber orientation detected in large PAs (Appendix A). Future measurements, including both mechanical ones in the circumferential and longitudinal directions and structural ones of collagen fiber orientation, will enable better quantification and modeling of anisotropy. Different properties of collagen in these two directions will affect the parameters (C_θ and C_z) and thus N. The effect of this assumption is unclear without additional experimental tests. Third, because the mechanical properties of pure elastin in mouse PA are not available, we assumed an isotropic neo-Hookean strain-energy function for elastin. While some studies found elastin in pig aorta to be isotropic [47,67], other studies found anisotropic properties of elastin in bovine aorta and rabbit facial vein [68,69]. Fourth, there is no accepted gold standard for determining the collagen transition point. Although the model-predicted collagen transition stretch is in good agreement with a previous estimation method and able to explain the experimentally observed arterial behavior, a direct measure of collagen transition stretch would allow validation of the model prediction. One promising approach for obtaining a direct measure is with in situ multi-photon microscopic imaging of arteries under various loads [60]. Fifth, the distinct contributions of the three arterial wall layers to the mechanical behavior were not measured and thus were not considered. Given that more collagen may predominantly exist

in the adventitial layer especially in this rodent model of PH, the collagen distribution and orientation may be different in the different arterial wall layers between control and PH states and it may be not appropriate to treat them the same as we have done here. All these limitations remain to be considered in future studies.

These limitations suggest future potential improvements to the model. For example, a model that captures the probability of collagen engagement [41,60,66,70], fraction of collagen fibers crosslinked, and the separate effects of the collagen subtypes and crosslink types could better describe the mechanical properties of arteries. Also, while the model as used here is appropriate when the collagen network is the main contributor to mechanical behavior and has the added advantage of separating the effects of collagen content from those of crosslinking, how well this model represents the physical structures and functions of collagen fibers remains unknown. Improvement of the model will be facilitated by investigation of the following mechanobiological questions: How exactly are the inner- and inter-molecular cross-links formed in collagen fibers? What are the tissue- and layer-specific collagen fiber alignments in healthy and diseased states and how do they change under load?

In summary, the present study used a microstructurally-based hyperelastic model and the neo-Hookean form to characterize the contributions of collagen and elastin respectively to arterial mechanics. The material parameters in the model were obtained by curve fitting to experimental, mechanical measurements of proximal PAs in a mouse model of HPH and these parameters correlated reasonably well to experimental biological measurements of collagen content and crosslinking. Modification of the model to incorporate a collagen engagement distribution probability function and measurement of other types of collagen crosslinking may improve these correlations. With the prediction of the collagen transition stretch, the model can elucidate the arterial wall structural characteristics responsible for arterial mechanical behavior observed experimentally. By linking the mechanical and biological properties, the model may allow us to predict biological changes during disease progression (e.g., pulmonary hypertension) from the measured mechanical behavior in patients. The applicability of this model to human PA mechanobiology remains to be determined.

Supplementary Material

Refer to Web version on PubMed Central for supplementary material.

Acknowledgments

References

1. Huang W, Sher YP, Delgado-West D, Wu JT, Peck K, Fung YC. Tissue remodeling of rat pulmonary artery in hypoxic breathing. I. Changes of morphology, zero-stress state, and gene expression. Ann Biomed Eng. 2001; 29:535–51. [PubMed: 11501619]

2. Poiani GJ, Tozzi CA, Yohn SE, Pierce RA, Belsky SA, Berg RA, et al. Collagen and elastin metabolism in hypertensive pulmonary arteries of rats. Circ Res. 1990; 66:968–78. [PubMed: 2317897]

3. Kobs RW, Muvarak NE, Eickhoff JC, Chesler NC. Linked mechanical and biological aspects of remodeling in mouse pulmonary arteries with hypoxia-induced hypertension. Am J Physiol Heart Circ Physiol. 2005; 288:H1209–17.10.1152/ajpheart.01129.2003 [PubMed: 15528223]

4. Lammers SR, Kao PH, Qi HJ, Hunter KS, Lanning C, Albietz J, et al. Changes in the structure-function relationship of elastin and its impact on the proximal pulmonary arterial mechanics of hypertensive calves. Am J Physiol Heart Circ Physiol. 2008; 295:H1451–9.10.1152/ajpheart. 00127.2008 [PubMed: 18660454]

5. Ooi CY, Wang Z, Tabima DM, Eickhoff JC, Chesler NC. The role of collagen in extralobar pulmonary artery stiffening in response to hypoxia-induced pulmonary hypertension. Am J Physiol Heart Circ Physiol. 2010; 299:H1823–31.10.1152/ajpheart.00493.2009 [PubMed: 20852040]

6. Drexler ES, Bischoff JE, Slifka AJ, McCowan CN, Quinn TP, Shandas R, et al. Stiffening of the extrapulmonary arteries from rats in chronic hypoxic pulmonary hypertension. J Res Natl Inst Stand Technol. 2008; 113:239–49.

7. Zhang Y, Dunn ML, Drexler ES, McCowan CN, Slifka AJ, Ivy DD, et al. A microstructural hyperelastic model of pulmonary arteries under normo- and hypertensive conditions. Ann Biomed Eng. 2005; 33:1042–52.10.1007/s10439-005-5771-2 [PubMed: 16133913]

8. Spann, JF. Contractile and pump function of the pressure-overloaded heart. In: Alpert, NR., editor. Perspect. Cardiovasc. Res. Vol 7. Myocard. Hypertrophy Fail. 1983. p. 19-38.

9. Durmowicz AG, Stenmark KR. Mechanisms of structural remodeling in chronic pulmonary hypertension. Pediatr Rev. 1999; 20:e91–102. [PubMed: 10551895]

10. Stenmark KR, Fagan KA, Frid MG. Hypoxia-induced pulmonary vascular remodeling: cellular and molecular mechanisms. Circ Res. 2006; 99:675–91.10.1161/01.RES.0000243584.45145.3f [PubMed: 17008597]

11. Voelkel NF, Quaife RA, Leinwand LA, Barst RJ, McGoon MD, Meldrum DR, et al. Right ventricular function and failure: report of a National Heart, Lung, and Blood Institute working group on cellular and molecular mechanisms of right heart failure. Circulation. 2006; 114:1883–91.10.1161/CIRCULATIONAHA.106.632208 [PubMed: 17060398]

12. Hunter KS, Lee P-F, Lanning CJ, Ivy DD, Kirby KS, Claussen LR, et al. Pulmonary vascular input impedance is a combined measure of pulmonary vascular resistance and stiffness and predicts clinical outcomes better than pulmonary vascular resistance alone in pediatric patients with pulmonary hypertension. Am Heart J. 2008; 155:166–74.10.1016/j.ahj.2007.08.014 [PubMed: 18082509]

13. Bogaard HJ, Abe K, Vonk Noordegraaf A, Voelkel NF. The right ventricle under pressure: cellular and molecular mechanisms of right-heart failure in pulmonary hypertension. Chest. 2009; 135:794–804.10.1378/chest.08-0492 [PubMed: 19265089]

14. Greyson CR. The right ventricle and pulmonary circulation: basic concepts. Rev Española Cardiol. 2010; 63:81–95.

15. Rodés-Cabau J, Domingo E, Román A, Majó J, Lara B, Padilla F, et al. Intravascular ultrasound of the elastic pulmonary arteries: a new approach for the evaluation of primary pulmonary hypertension. Heart. 2003; 89:311–5. [PubMed: 12591838]

16. Mahapatra S, Nishimura RA, Sorajja P, Cha S, McGoon MD. Relationship of pulmonary arterial capacitance and mortality in idiopathic pulmonary arterial hypertension. J Am Coll Cardiol. 2006; 47:799–803.10.1016/j.jacc.2005.09.054 [PubMed: 16487848]

17. Mahapatra S, Nishimura RA, Oh JK, McGoon MD. The prognostic value of pulmonary vascular capacitance determined by Doppler echocardiography in patients with pulmonary arterial

hypertension. J Am Soc Echocardiogr. 2006; 19:1045–50.10.1016/j.echo.2006.03.008 [PubMed: 16880101]

18. Gan CT-J, Lankhaar J-W, Westerhof N, Marcus JT, Becker A, Twisk JWR, et al. Noninvasively assessed pulmonary artery stiffness predicts mortality in pulmonary arterial hypertension. Chest. 2007; 132:1906–12.10.1378/chest.07-1246 [PubMed: 17989161]

19. Stevens GR, Garcia-Alvarez A, Sahni S, Garcia MJ, Fuster V, Sanz J. RV dysfunction in pulmonary hypertension is independently related to pulmonary artery stiffness. JACC Cardiovasc Imaging. 2012; 5:378–87.10.1016/j.jcmg.2011.11.020 [PubMed: 22498327]

20. Su Z, Hunter KS, Shandas R. Impact of pulmonary vascular stiffness and vasodilator treatment in pediatric pulmonary hypertension: 21 patient-specific fluid-structure interaction studies. Comput Methods Programs Biomed. 2012; 108:617–28.10.1016/j.cmpb.2011.09.002 [PubMed: 21975085]

21. Kao PH, Lammers SR, Tian L, Hunter K, Stenmark KR, Shandas R, et al. A microstructurally driven model for pulmonary artery tissue. J Biomech Eng. 2011; 133:051002.10.1115/1.4002698 [PubMed: 21599093]

22. Tian L, Chesler NC. In vivo and in vitro measurements of pulmonary arterial stiffness: A brief review. Pulm Circ. 2012; 2:505–17.10.4103/2045-8932.105040 [PubMed: 23372936]

23. Wang Z, Lakes RS, Eickhoff JC, Chesler NC. Effects of collagen deposition on passive and active mechanical properties of large pulmonary arteries in hypoxic pulmonary hypertension. Biomech Model Mechanobiol. 2013; 12:1115–25.10.1007/s10237-012-0467-7 [PubMed: 23377784]

24. Tabima DM, Chesler NC. The effects of vasoactivity and hypoxic pulmonary hypertension on extralobar pulmonary artery biomechanics. J Biomech. 2010; 43:1864–9.10.1016/j.jbiomech. 2010.03.033 [PubMed: 20416876]

25. Roach MR, Burton AC. The reason for the shape of the distensibility curves of arteries. Can J Biochem Physiol. 1957; 35:681–90. [PubMed: 13460788]

26. Holzapfel GA, Gasser TC, Ogden RW. A New Constitutive Framework for Arterial Wall Mechanics and a Comparative Study of Material Models. J Elast. 2000; 61:1–48.10.1023/A: 1010835316564

27. Tian L, Lammers SR, Kao PH, Albietz JA, Stenmark KR, Qi HJ, et al. Impact of residual stretch and remodeling on collagen engagement in healthy and pulmonary hypertensive calf pulmonary arteries at physiological pressures. Ann Biomed Eng. 2012; 40:1419–33.10.1007/ s10439-012-0509-4 [PubMed: 22237861]

28. Tozzi CA, Christiansen DL, Poiani GJ, Riley DJ. Excess collagen in hypertensive pulmonary arteries decreases vascular distensibility. Am J Respir Crit Care Med. 1994; 149:1317–26. [PubMed: 8173773]

29. Wang Z, Chesler NC. Role of collagen content and cross-linking in large pulmonary arterial stiffening after chronic hypoxia. Biomech Model Mechanobiol. 2012; 11:279–89.10.1007/ s10237-011-0309-z [PubMed: 21538012]

30. Cox RH, Bashey R, Jimenez S. Effects of chronic beta-aminoproprionitrile treatment on rat carotid artery. Blood Vessels. 1988; 25:53–62. [PubMed: 3345350]

31. Norton GR, Tsotetsi J, Trifunovic B, Hartford C, Candy GP, Woodiwiss AJ. Myocardial stiffness is attributed to alterations in cross-linked collagen rather than total collagen or phenotypes in spontaneously hypertensive rats. Circulation. 1997; 96:1991–8. [PubMed: 9323091]

32. Brüel A, Ortoft G, Oxlund H. Inhibition of cross-links in collagen is associated with reduced stiffness of the aorta in young rats. Atherosclerosis. 1998; 140:135–45. [PubMed: 9733224]

33. Badenhorst D, Maseko M, Tsotetsi OJ, Naidoo A, Brooksbank R, Norton GR, et al. Cross-linking influences the impact of quantitative changes in myocardial collagen on cardiac stiffness and remodelling in hypertension in rats. Cardiovasc Res. 2003; 57:632–41. [PubMed: 12618225]

34. López B, Querejeta R, González A, Larman M, Díez J. Collagen cross-linking but not collagen amount associates with elevated filling pressures in hypertensive patients with stage C heart failure: potential role of lysyl oxidase. Hypertension. 2012; 60:677–83.10.1161/ HYPERTENSIONAHA.112.196113 [PubMed: 22824984]

35. Fratzl, P. Collagen: Structure and Mechanics. New York: Springer; 2008.

36. Vaishnav RN, Young JT, Patel DJ. Distribution of stresses and of strain-energy density through the wall thickness in a canine aortic segment. Circ Res. 1973; 32:577–83. [PubMed: 4713199]

37. Humphrey JD. Mechanics of the arterial wall: review and directions. Crit Rev Biomed Eng. 1995; 23:1–162. [PubMed: 8665806]

38. Fung YC, Fronek K, Patitucci P. Pseudoelasticity of arteries and the choice of its mathematical expression. Am J Physiol. 1979; 237:H620–31. [PubMed: 495769]

39. Takamizawa K, Hayashi K. Strain energy density function and uniform strain hypothesis for arterial mechanics. J Biomech. 1987; 20:7–17. [PubMed: 3558431]

40. Holzapfel GA, Weizsäcker HW. Biomechanical behavior of the arterial wall and its numerical characterization. Comput Biol Med. 1998; 28:377–92. [PubMed: 9805198]

41. Zulliger MA, Fridez P, Hayashi K, Stergiopulos N. A strain energy function for arteries accounting for wall composition and structure. J Biomech. 2004; 37:989–1000.10.1016/j.jbiomech. 2003.11.026 [PubMed: 15165869]

42. Arruda EM, Boyce MC. A three-dimensional constitutive model for the large stretch behavior of rubber elastic materials. J Mech Phys Solids. 1993; 41:389–412.10.1016/0022-5096(93)90013-6

43. Bischoff JE, Arruda EM, Grosh K. A Microstructurally Based Orthotropic Hyperelastic Constitutive Law. J Appl Mech. 2002; 69:570–9.10.1115/1.1485754

44. Chuong CJ, Fung YC. On residual stresses in arteries. J Biomech Eng. 1986; 108:189–92. [PubMed: 3079517]

45. Han HC, Fung YC. Direct measurement of transverse residual strains in aorta. Am J Physiol. 1996; 270:H750–9. [PubMed: 8779853]

46. Watton PN, Ventikos Y, Holzapfel GA. Modelling the mechanical response of elastin for arterial tissue. J Biomech. 2009; 42:1320–5.10.1016/j.jbiomech.2009.03.012 [PubMed: 19394942]

47. Gundiah N, Ratcliffe MB, Pruitt LA. The biomechanics of arterial elastin. J Mech Behav Biomed Mater. 2009; 2:288–96.10.1016/j.jmbbm.2008.10.007 [PubMed: 19627833]

48. Bischoff J, Arruda E, Grosh K. A new constitutive model for the compressibility of elastomers at finite deformations. Rubber Chem Technol. 2001; 74:541–59.

49. Anand L. A constitutive model for compressible elastomeric solids. Comput Mech. 1996; 18:339–55.10.1007/BF00376130

50. Treloar LRG, Riding G. A Non-Gaussian Theory for Rubber in Biaxial Strain. I. Mechanical Properties. Proc R Soc A Math Phys Eng Sci. 1979; 369:261–80.10.1098/rspa.1979.0163

51. Chen X, Nadiarynkh O, Plotnikov S, Campagnola PJ. Second harmonic generation microscopy for quantitative analysis of collagen fibrillar structure. Nat Protoc. 2012; 7:654–69.10.1038/nprot. 2012.009 [PubMed: 22402635]

52. Bredfeldt JS, Liu Y, Pehlke CA, Conklin MW, Szulczewski JM, Inman DR, et al. Computational segmentation of collagen fibers from second-harmonic generation images of breast cancer. J Biomed Opt. 2014; 19:16007.10.1117/1.JBO.19.1.016007 [PubMed: 24407500]

53. Cameron, AC.; Trivedi, PK. Regression analysis of count data. Cambridge, UK; New York, NY, USA: Cambridge University Press; 1998.

54. Kuhn W, Grün F. Beziehungen zwischen elastischen Konstanten und Dehnungsdoppelbrechung hochelastischer Stoffe. Kolloid-Zeitschrift. 1942; 101:248–71.10.1007/BF01793684

55. Reusser M, Hunter KS, Lammers SR, Stenmark KR. Validation of a pressure diameter method for determining modulus and strain of collagen engagement for long branches of bovine pulmonary arteries. J Biomech Eng. 2012; 134:054501.10.1115/1.4006686 [PubMed: 22757496]

56. Coleman, HW.; Steele, WG. Experimentation and Uncertainty Analysis for Engineers. New York: Wiley; 1999.

57. Efron B, Tibshirani R. Bootstrap methods for standard errors, confidence intervals, and other measures of statistical accuracy. Stat Sci. 1986; 1:54–75.

58. Bland JM, Altman DG. Statistical methods for assessing agreement between two methods of clinical measurement. Lancet. 1986; 1:307–10. [PubMed: 2868172]

59. Taylor R. Interpretation of the Correlation Coefficient: A Basic Review. J Diagnostic Med Sonogr. 1990; 6:35–9.10.1177/875647939000600106

60. Hill MR, Duan X, Gibson GA, Watkins S, Robertson AM. A theoretical and nondestructive experimental approach for direct inclusion of measured collagen orientation and recruitment into

mechanical models of the artery wall. J Biomech. 2012; 45:762–71.10.1016/j.jbiomech. 2011.11.016 [PubMed: 22305290]

61. Finlay HM, McCullough L, Canham PB. Three-dimensional collagen organization of human brain arteries at different transmural pressures. J Vasc Res. 32:301–12. [PubMed: 7578798]

62. Canham PB, Whittaker P, Barwick SE, Schwab ME. Effect of pressure on circumferential order of adventitial collagen in human brain arteries. Can J Physiol Pharmacol. 1992; 70:296–305. [PubMed: 1521182]

63. Pfeiffer BJ, Franklin CL, Hsieh F, Bank RA, Phillips CL. Alpha 2(I) collagen deficient oim mice have altered biomechanical integrity, collagen content, and collagen crosslinking of their thoracic aorta. Matrix Biol. 2005; 24:451–8.10.1016/j.matbio.2005.07.001 [PubMed: 16095890]

64. Liu X, Wu H, Byrne M, Jeffrey J, Krane S, Jaenisch R. A targeted mutation at the known collagenase cleavage site in mouse type I collagen impairs tissue remodeling. J Cell Biol. 1995; 130:227–37. [PubMed: 7790374]

65. Eyre, DR.; Wu, J-J. Collagen Cross-Links. In: Brinckmann, J.; Notbohm, H.; Muller, PK., editors. Top Curr Chem. 2005. p. 207-29.

66. Roy S, Boss C, Rezakhaniha R, Stergiopulos N. Experimental characterization of the distribution of collagen fiber recruitment. J Biorheol. 2010; 24:84–93.

67. Gundiah N, Ratcliffe MB, Pruitt LA. Determination of strain energy function for arterial elastin: Experiments using histology and mechanical tests. J Biomech. 2007; 40:586–94.10.1016/ j.jbiomech.2006.02.004 [PubMed: 16643925]

68. Zou Y, Zhang Y. An experimental and theoretical study on the anisotropy of elastin network. Ann Biomed Eng. 2009; 37:1572–83.10.1007/s10439-009-9724-z [PubMed: 19484387]

69. Rezakhaniha R, Stergiopulos N. A structural model of the venous wall considering elastin anisotropy. J Biomech Eng. 2008; 130:031017.10.1115/1.2907749 [PubMed: 18532866]

70. Zulliger MA, Rachev A, Stergiopulos N. A constitutive formulation of arterial mechanics including vascular smooth muscle tone. Am J Physiol Heart Circ Physiol. 2004; 287:H1335–43.10.1152/ajpheart.00094.2004 [PubMed: 15130890]
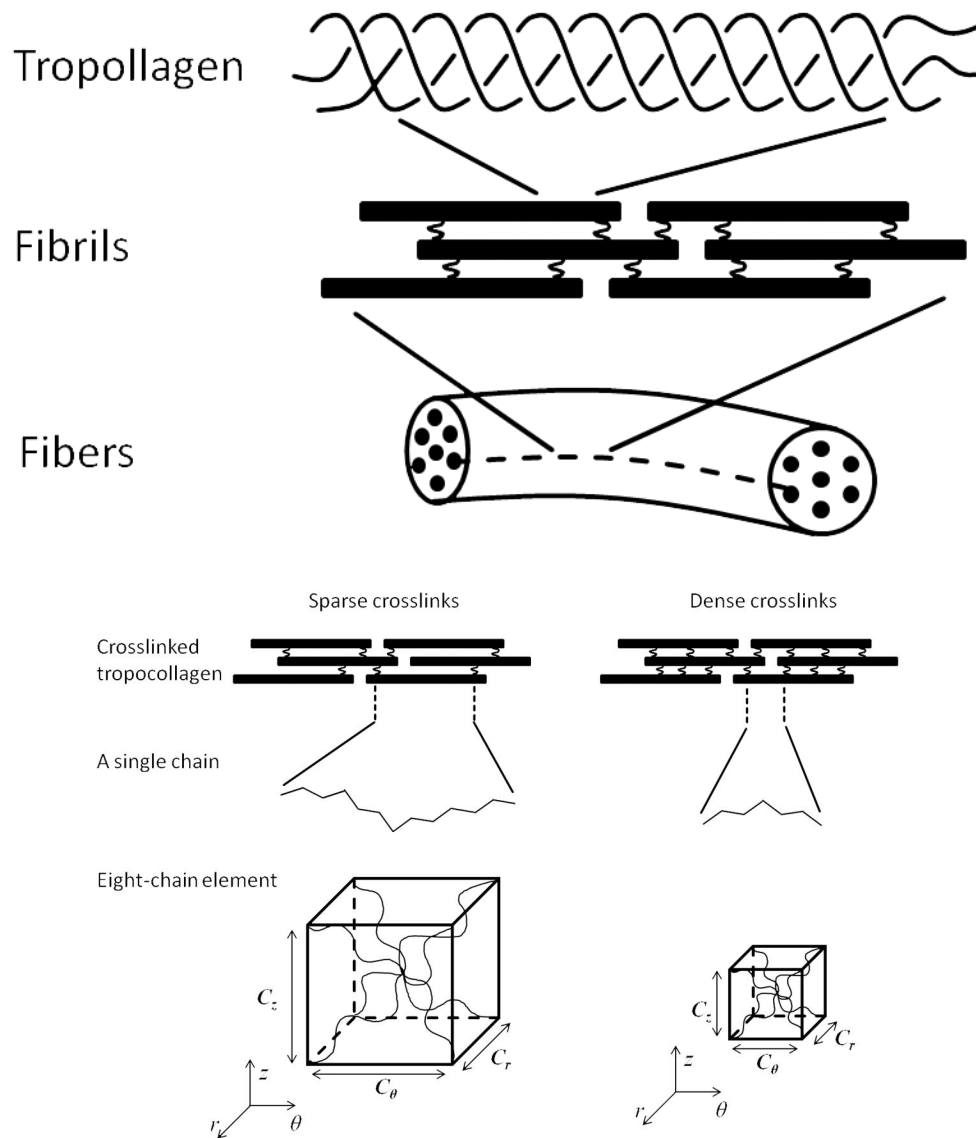
Figure 1.
(A) Schematic of tropocollagen and its assembly to collagen fibrils and fibers (adapted from Fratzl 2008). Crosslinks are indicated by spring-like connectors between tropocollagen molecules; (B) Representative models of sparsely and densely crosslinked tropocollagen. Note that a single chain in the eight-chain model represents the section of tropocollagen molecule between neighboring crosslinks. This single chain is made up of multiple subunits with fixed length, which represent the repeating amino acid motif on a tropocollagen molecule. The length of each chain in the eight-chain element depends on the number of subunits, which in turn depends on the density of crosslinks. The element has normalized dimensions $C_r \times C_\theta \times C_z$ along the material axes r, θ, z, respectively.

Figure 2A
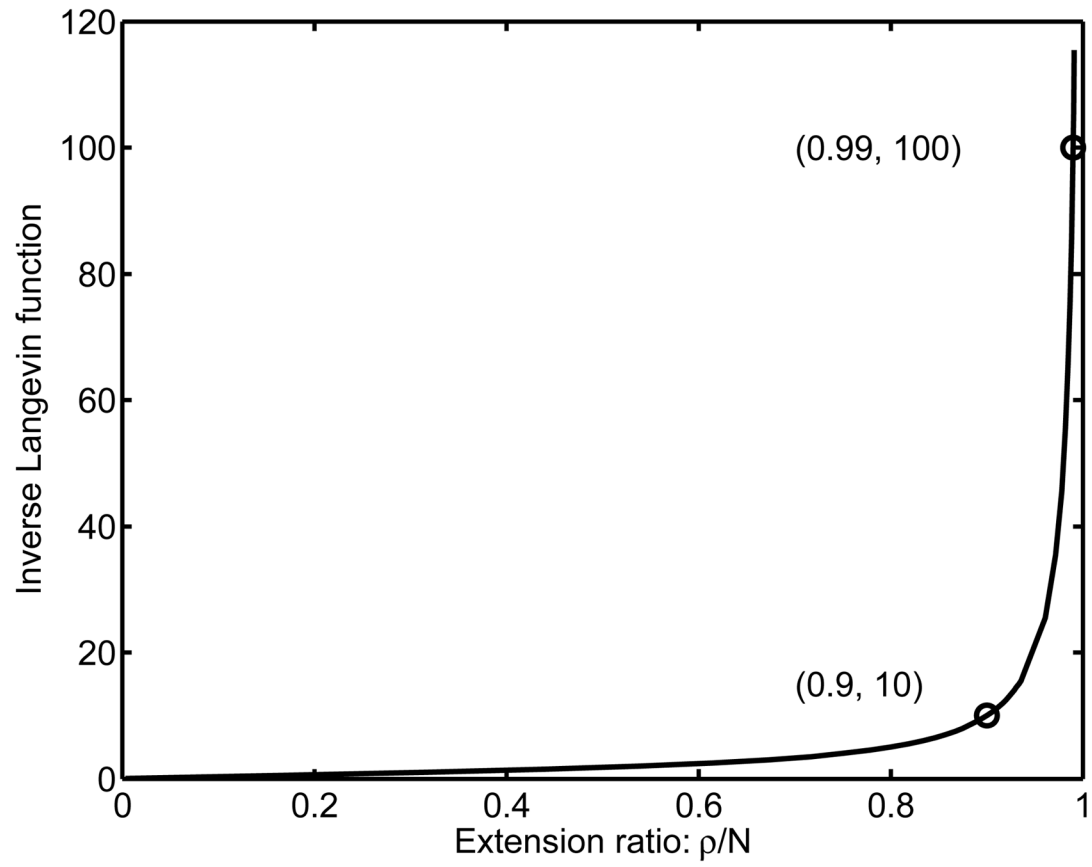
Figure 2B
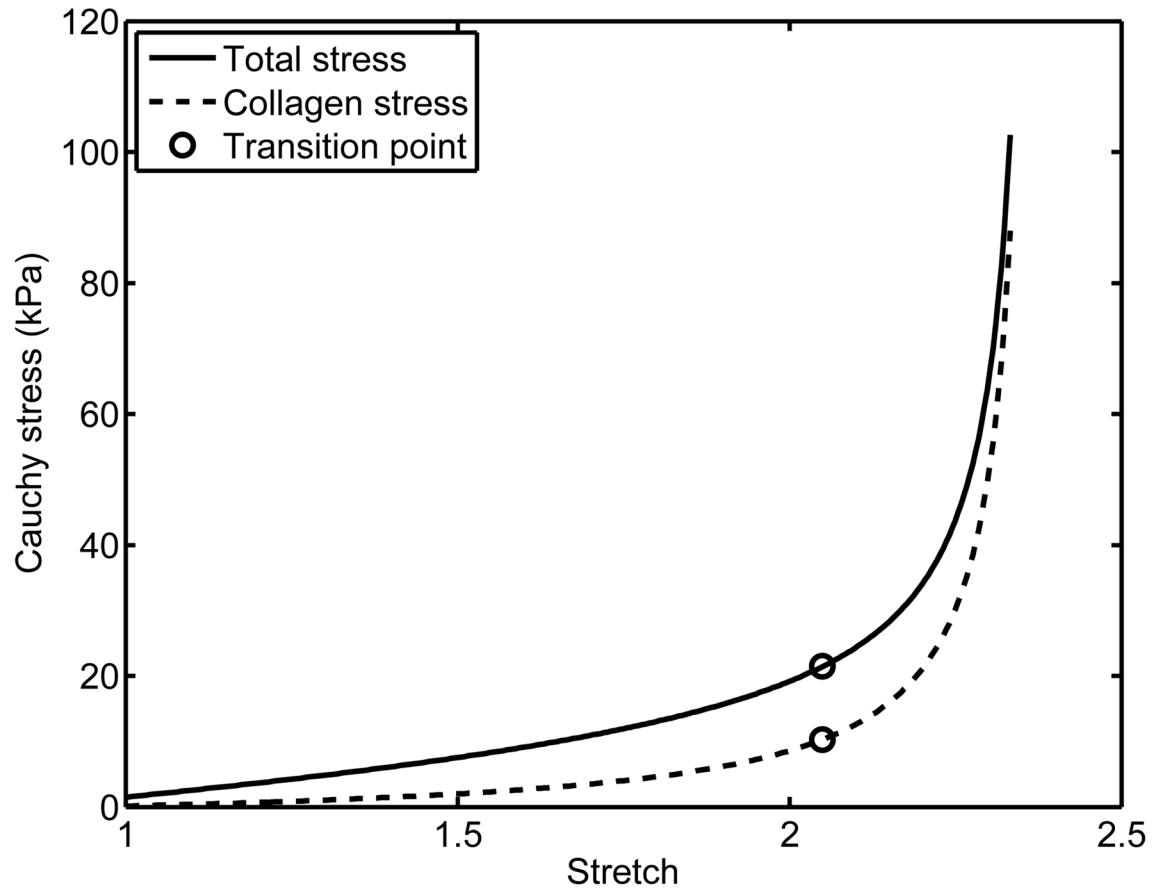
Figure 2.
(A) Plot of the inverse Langevin function versus the chain extension ratio (ρ/N). Around ρ/N = 0.9, the value of the function starts to increase dramatically with ρ/N. (B) Representative Cauchy stress-stretch curve for artery and collagen only and the transition point as predicted from model.
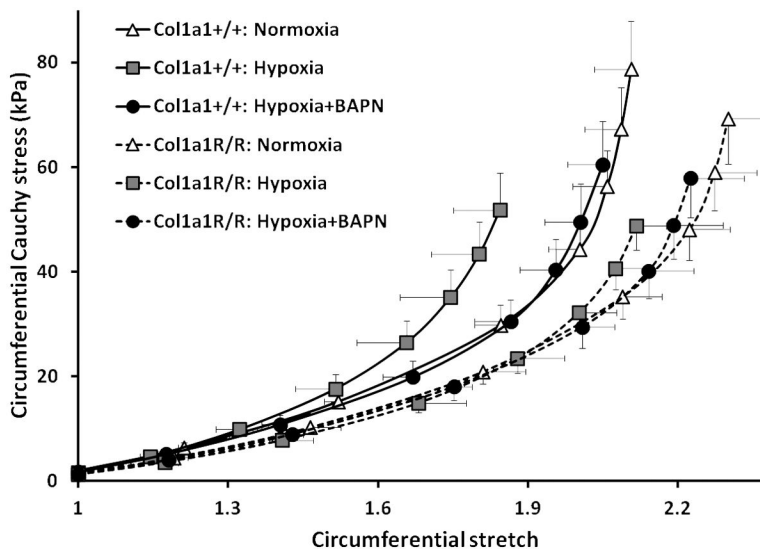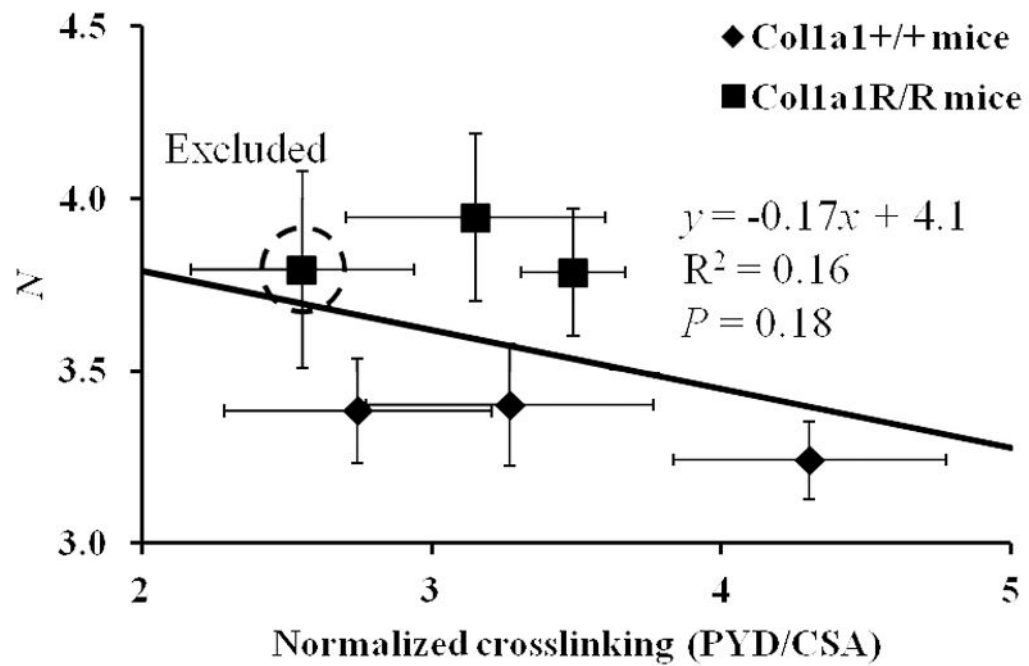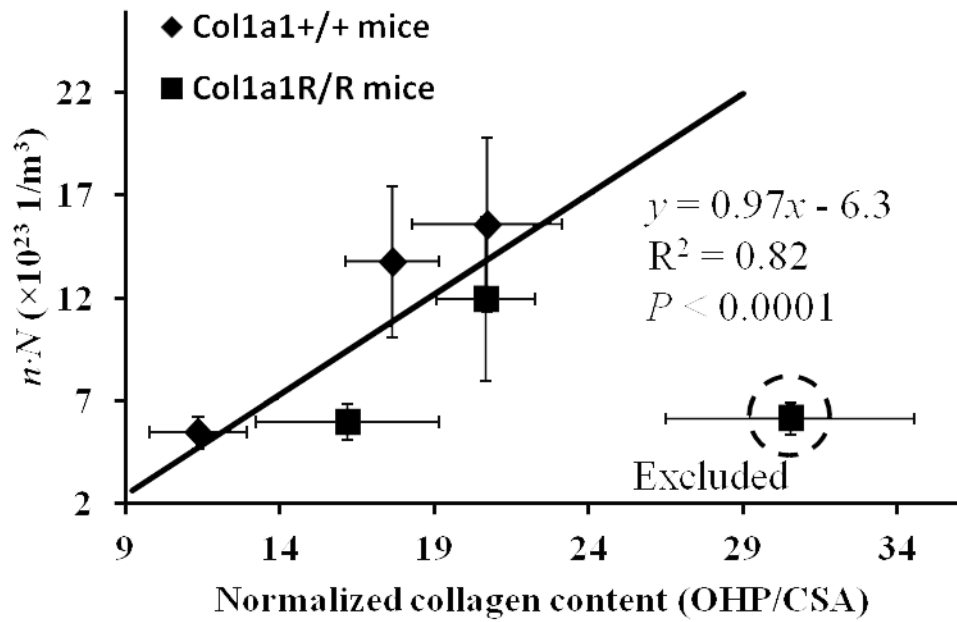
Figure 3.
Average experimentally obtained circumferential Cauchy stress-stretch curves of all groups. The stress and stretch of all the arteries in a group at a pressure during the inflation test (e.g., 5, 10 mmHg) were averaged separately. Col1a1$^{+/+}$ mice: solid lines; Col1$^{R/R}$ mice: dotted lines.
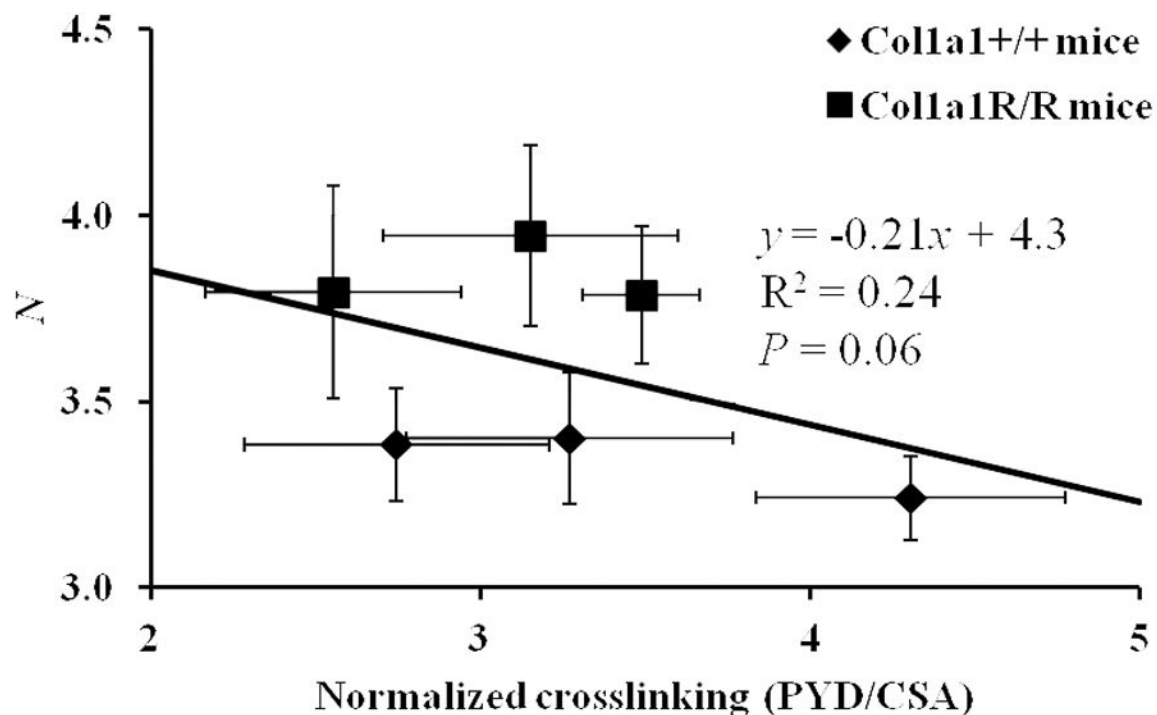
Figure 4.
Group correlations (A) between normalized collagen content (OHP/CSA) and material parameter ($n \cdot N$) and (B) & (C) between normalized crosslinking (PYD/CSA) and material parameter (N). Note that Col1a1$^{R/R}$ Hypoxia+BAPN group (surrounded by a circle) is excluded for the trend lines plotted in (A) and (B) with the corresponding correlation coefficient. A moderate correlation is found either (B) with or (C) without Col1a1$^{R/R}$ Hypoxia+BAPN group excluded in the correlation analysis.
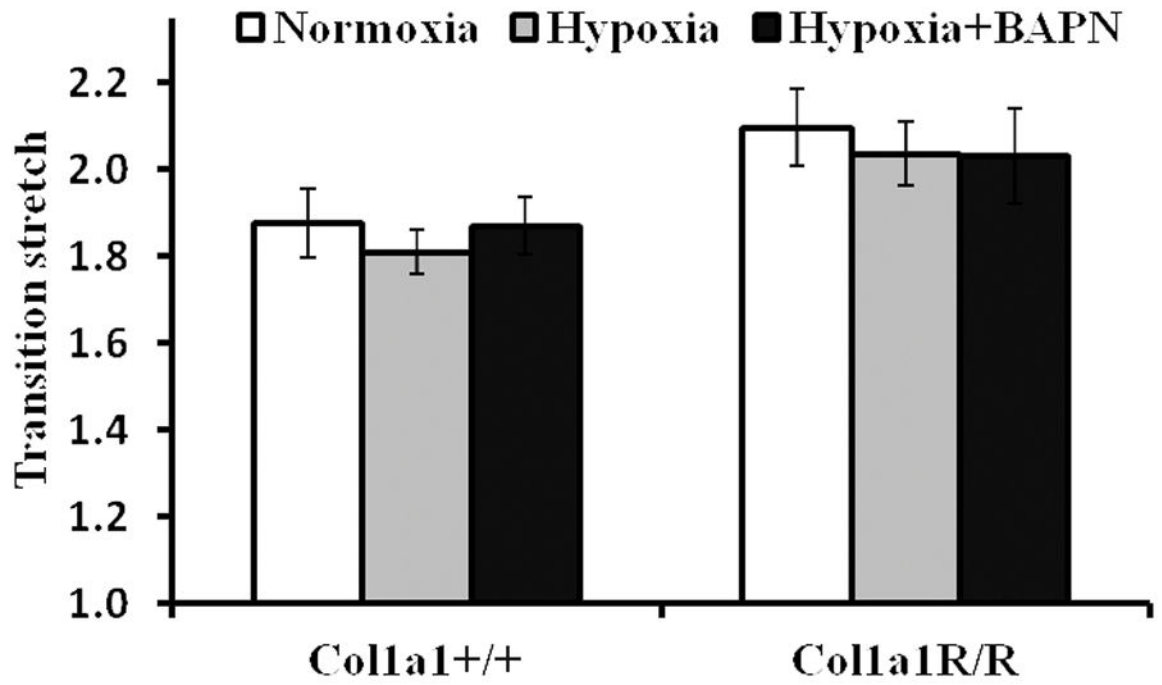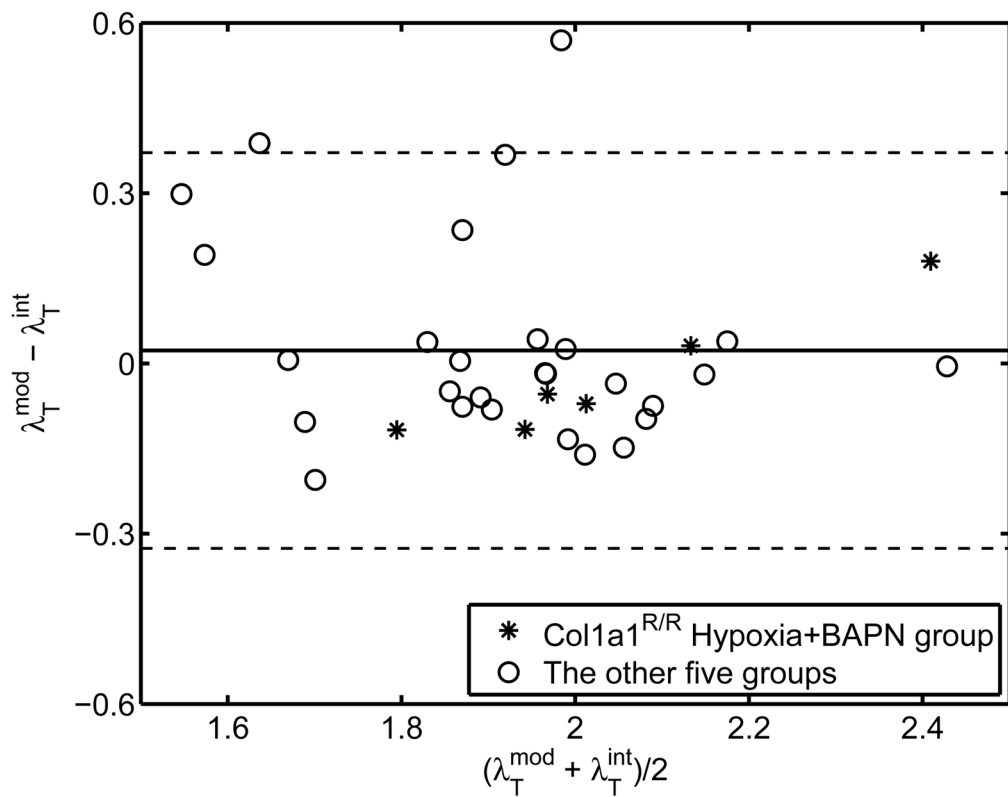
Figure 5B

Figure 5.

(A) Collagen transition stretch predicted from model for all six groups; (B) Bland-Altman agreement analysis between the transition stretch estimated from the model ($\lambda_{\mathrm{T}}^{\mathrm{mod}}$) and the method using the intersection of two linear lines ($\lambda_{\mathrm{T}}^{\mathrm{ind}}$).
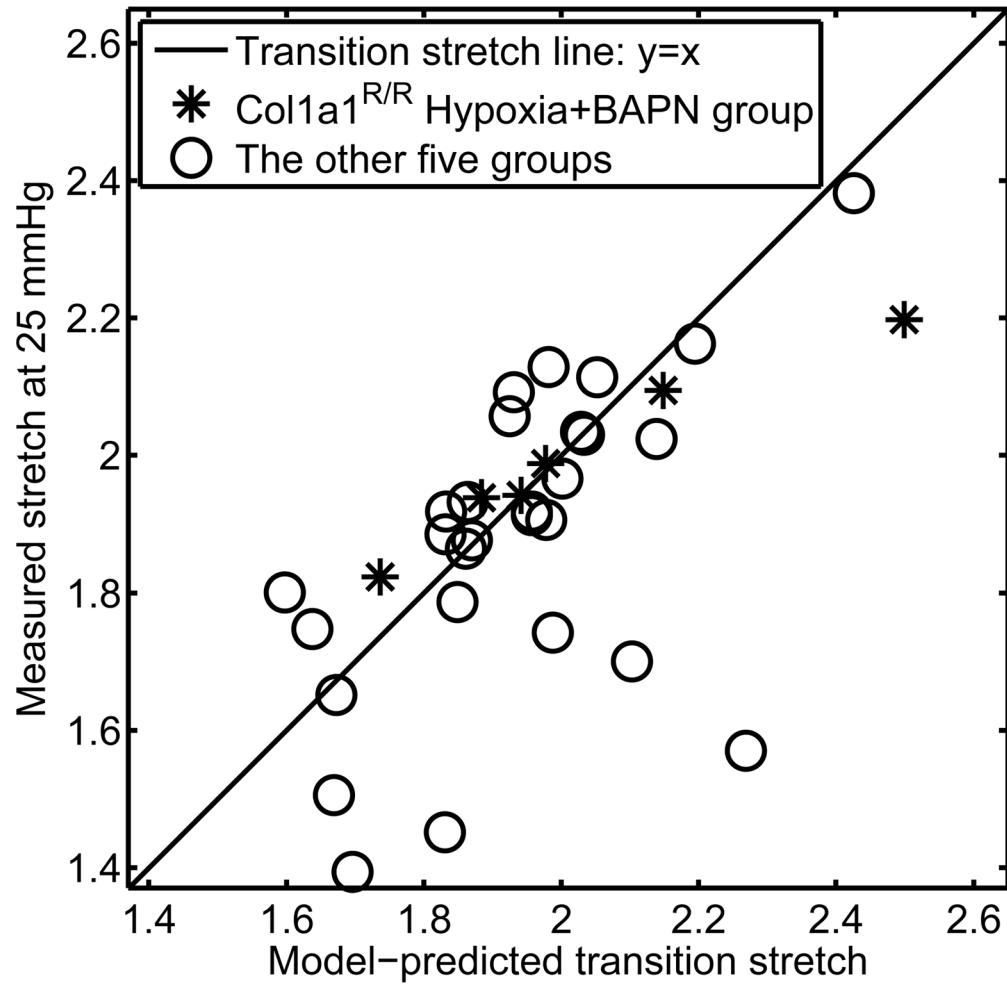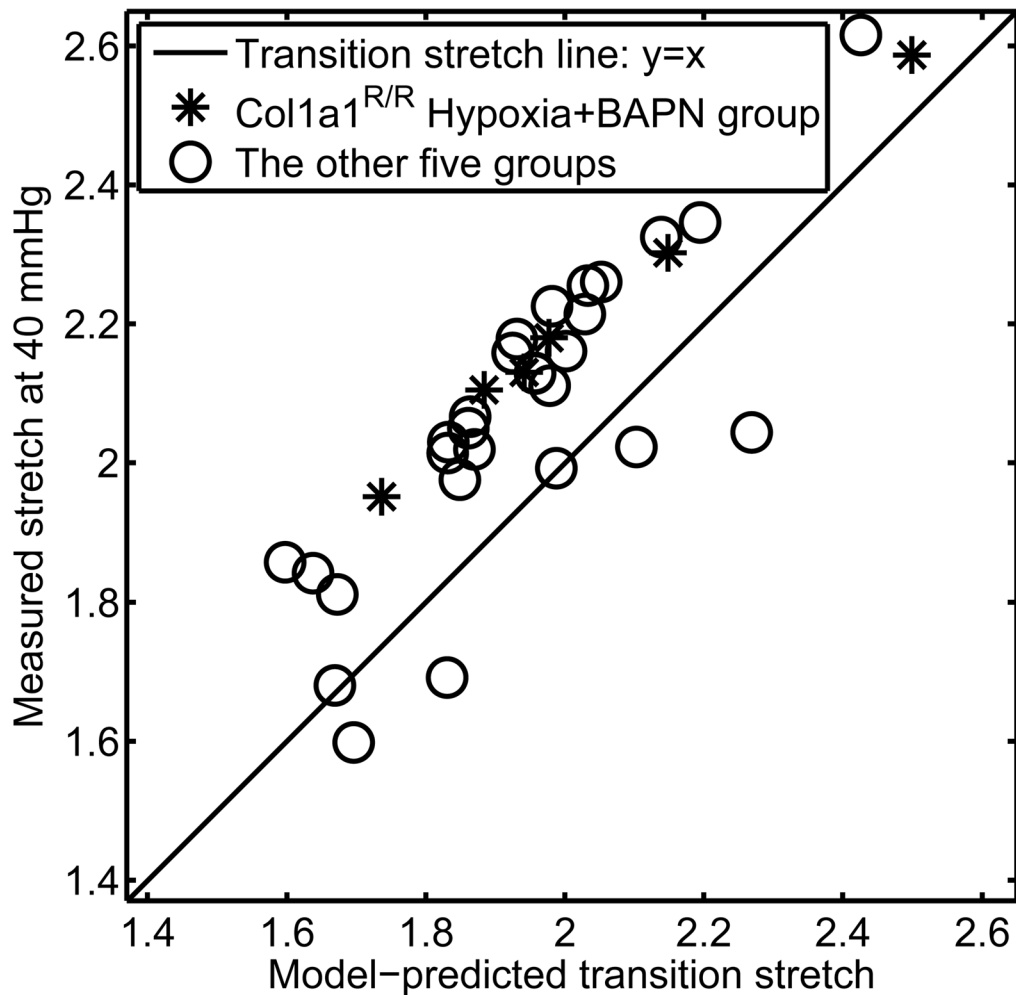
Figure 6A

Figure 6B

Figure 6.
Comparison of model-predicted transition stretch and the experimental circumferential stretch of LPA at (A) 25 mmHg and (B) 40 mmHg obtained from the inflation test. The transition stretch line (i.e., equality line) is given. Below this line, the collagen fibers are predicted not to engage; while above this line, the collagen fibers are predicted to be already engaged.
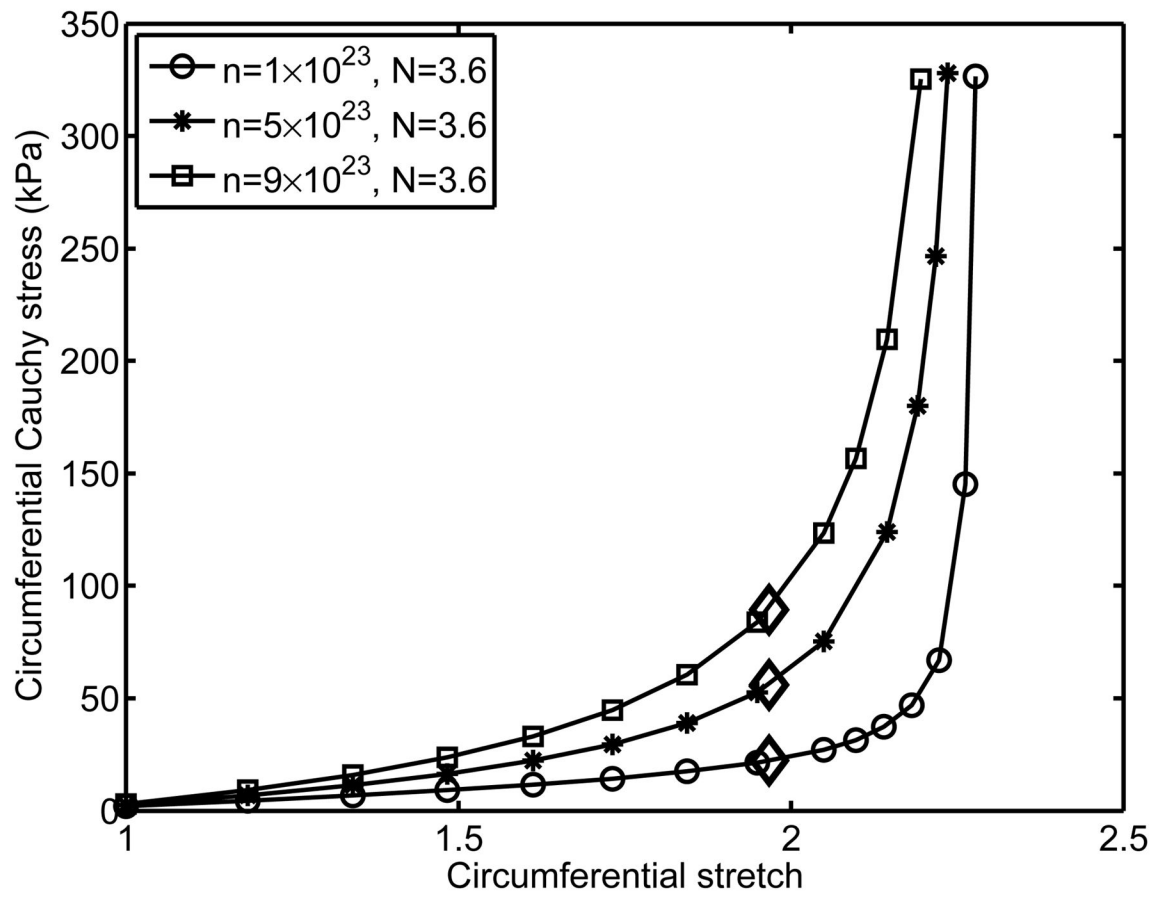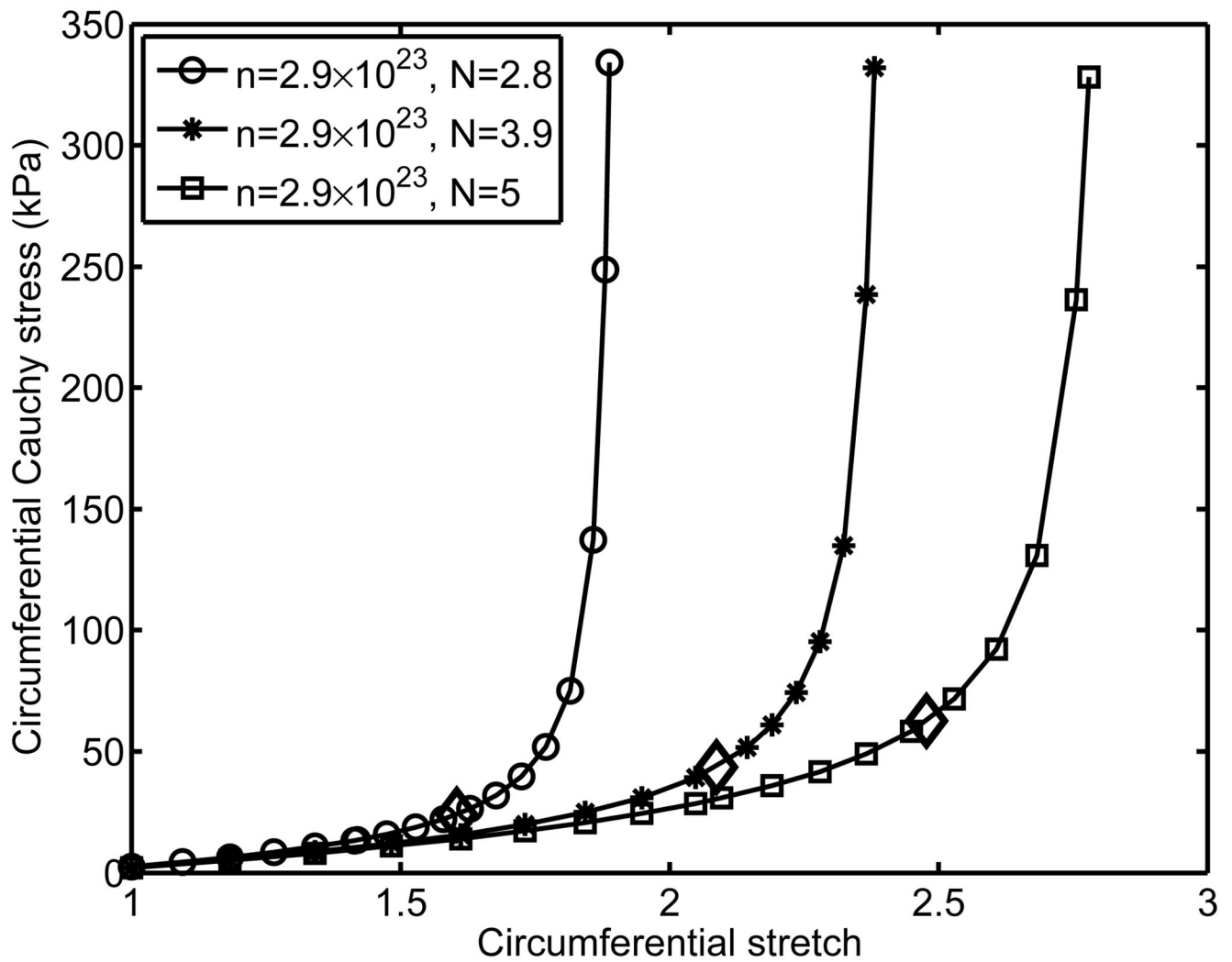
Figure 7A

Figure 7B

Figure 7.
Effect of (A) the chain density (*n*) and (B) the number of subunits in each chain (*N*) on the circumferential stress-stretch relationship. In the simulation, the material parameter for elastin G = 3.7 kPa and the longitudinal stretch λ_z = 1.4. The transition stretch λ_T^{mod}=1.97 for all three cases in (A), while in (B) λ_T^{mod}=1.60, 2.09, and 2.48 for N = 2.8, 3.9 and 5.0, respectively.

Table 1

Summary of cross-sectional area (CSA) of left pulmonary artery (LPA), and normalized collagen content (OHP) and crosslinking (PYD).

Strain	Treatment	CSA (mm^2)	OHP/CSA (ug/mm^2 ·vessel)	PYD/CSA (nmol/mm^2 · vessel)
Col1a1$^{+/+}$	Normoxia	0.079±0.009	11.4±1.6	3.3±0.5
	Hypoxia	0.082±0.008	20.7±2.4[*]	4.3±0.5
	Hypoxia +BAPN	0.079±0.005	17.6±1.5[*]	2.8±0.5[#]
Col1a1$^{R/R}$	Normoxia	0.074±0.010	16.2±3.0	3.2±0.5
	Hypoxia	0.087±0.003	20.7±1.6	3.5±0.2
	Hypoxia +BAPN	0.085±0.008	30.5±4.0[*#]	2.6±0.4[#]

Values are mean ± SE. Number of samples for each group is 3~7.

[*] $P < 0.05$ for Hypoxia or Hypoxia+BAPN vs. Normoxia;

[#] $P < 0.05$ for Hypoxia+BAPN vs. Hypoxia. Note that OHP and CSA were measured on left pulmonary artery (LPA) and PYD was measured on right pulmonary artery (RPA).

Author Manuscript

Author Manuscript

Author Manuscript

Author Manuscript

Table 2

Summary of material parameters in the arterial constitutive model.

Strain	Treatment	G (kPa)	$C_\theta = C_z$	C_r	$n \times 10^{23}$ (1/m³)	N	$n \cdot N \times 10^{23}$ (1/m³)
Col1a1$^{+/+}$	Normoxia	5.7 ± 1.3	2.6 ± 0.1	0	1.6 ± 0.2	3.4 ± 0.2	5.5 ± 0.8
	Hypoxia	2.4 ± 0.8	2.5 ± 0.1	0	4.9 ± 1.4	3.2 ± 0.1	15.6 ± 4.2
	Hypoxia+BAPN	3.0 ± 0.9	2.6 ± 0.4	0	4.3 ± 1.3	3.4 ± 0.2	13.8 ± 3.7
Col1a1$^{R/R}$	Normoxia	4.8 ± 0.9	2.8 ± 0.1	0	1.6 ± 0.3	3.9 ± 0.2	6.0 ± 0.9
	Hypoxia	2.8 ± 0.6	2.7 ± 0.1	0	3.0 ± 0.9	3.8 ± 0.2	12.0 ± 4.0
	Hypoxia+BAPN	4.0 ± 0.8	2.7 ± 0.1	0	1.6 ± 0.1	3.8 ± 0.3	6.2 ± 0.8

Values are mean ± SE. Number of samples for each group is 5~6. Parameter C_r is set to be zero.